Oort cloud Ecology: II. the chronology of the formation of the Oort cloud

Portegies Zwart, S.F.; Torres Rodriguez, S.; Cai, M.X.; Brown, A.G.A.

Astronomy & Astrophysics manuscript no. OortCloud
October 14, 2021

Oort cloud Ecology II: The chronology of the formation of the Oort cloud

Simon Portegies Zwart[1], Santiago Torres[1,2], Maxwell X. Cai[1] and Anthony G. A. Brown[1],

[1] Leiden Observatory, Leiden University, PO Box 9513, 2300 RA, Leiden, The Netherlands
[2] Department of Physics and Astronomy, University of California, Los Angeles, CA 90095, USA

October 14, 2021

ABSTRACT

Jan Hendrik Oort hypothesized, based on a spike in the reciprocal orbital separation at $1/a \lesssim 10^{-4}\,\mathrm{au}^{-1}$, the existence of a distant cloud of cometary objects that orbit the Sun. The Oort cloud is the source of long-period comets, but it is not observed directly, and its origin remains theoretical. Theories on its origin postulate a sequence of events that are tested individually but never as a consistent chronology.

We present a chronology on the formation and early evolution of the Oort cloud, and test the sequence of events by simulating the formation process in subsequent amalgamated steps. These simulations start with the Solar system being born with planets and asteroids in a stellar cluster orbiting the Galactic center. Upon ejection from its birth environment, we continue to follow the Solar system's evolution while it sojourns the Galaxy as an isolated planetary system.

We conclude that the range in semi-major axis between $\sim 100\,\mathrm{au}$ and several $\sim 10^3\,\mathrm{au}$ still bears the signatures of the Sun being born in a $\gtrsim 1000\,M_\odot/\mathrm{pc}^3$ star cluster, and that most of the outer Oort cloud formed after the Solar system escaped. The escape, we argue, happened between $\sim 20\,\mathrm{Myr}$ and $50\,\mathrm{Myr}$ after birth of the Solar system.

Today, the bulk of the material in the Oort cloud ($\sim 70\%$) originates from the region in the circumstellar disk that was located between $\sim 15\,\mathrm{au}$ and $\sim 35\,\mathrm{au}$, near the current location of the ice-giants and the Centaur family of asteroids. This population is eradicated if the ice-giant planets were born in orbital resonance. Planet migration or chaotic orbital reorganization, occurring while the Solar system is still a cluster member is, according to our model, inconsistent with the presence of the Oort cloud. About half the inner Oort cloud, between 100 and $10^4\,\mathrm{au}$, and a quarter of the material in the outer Oort cloud $\gtrsim 10^4\,\mathrm{au}$ could be non-native to the Solar system but was captured from free-floating derbis in the cluster or from the circumstellar disk of other stars in the birth cluster. Characterizing this population will help us to reconstruct the Solar system's history.

1. Introduction

1.1. A brief history on the formation of the Solar system

The formation of the Oort cloud (Oort 1950) requires a sequence of events on temporal and spatial scales that span more than 8 orders of magnitude, from the Solar system (on scales of years and au) to the entire Galaxy (on Gyr and kpc scales). As a consequence, the formation of the Oort cloud was not a simple happening; Occam's razor does not seem to apply here.

Individual events that led to the formation of the Oort cloud have in the past been modeled separately to explain specific features (see e.g. Hayashi et al. 1985; Dones et al. 2004a; Higuchi et al. 2007; Lykawka & Mukai 2008; Leto et al. 2008; Paulech et al. 2010; Rickman 2014; Dones et al. 2015; Fouchard et al. 2018). The chain of events, however, has never been tested as a causal sequence. We present the results of computer simulations designed to model a chronology of the formation of the Oort cloud in which individual processes are included at their proper scales. Each phase is simulated precisely and connected to the next stage of the cascade. By doing so, we construct a consistent picture of the formation and early evolution of the Oort cloud.

In our analysis, we assume that the Solar system formed, like most stars (Lada & Lada 2003; Adams 2010), in a giant molecular cloud in which gas contracts under its own gravity, and stars form with disks around them (Beckwith et al. 1990; McKee & Ostriker 2007; Gavagnin et al. 2017). The Solar system then probably formed in a cluster of stars which interacted mutually before the Sun escaped the cluster (Portegies Zwart et al. 2009). The circumstellar disk, a leftover from the star-formation process, led to the coagulation of planets (Kokubo & Ida 1998; Kokubo & Ida 2002; Kenyon & Bromley 2006; Wyatt 2008; Levison et al. 2010b; Williams & Cieza 2011; Emsenhuber et al. 2020a,b; Schlecker et al. 2020) and a large number of planetesimals (Johansen et al. 2007; Johansen & Lambrechts 2017; Popovas et al. 2018; Johansen et al. 2021)[1]. The presence of nearby stars in the parent cluster will have affected the morphology of the gaseous disk through tidal perturbations (Clarke & Pringle 1993; Pfalzner et al. 2005; Winter et al. 2018; Cuello et al. 2019), photo-evaporation (Johnstone et al. 1998; Adams et al. 2004; Clarke 2007), and stellar winds (Offner & Arce 2015).

The evolution of the circumstellar disk has profound consequences for the newly formed planetary orbits (Laughlin & Adams 1998; Breslau et al. 2014; Vincke et al. 2015; Vincke & Pfalzner 2016; Concha-Ramírez et al. 2021). Although at the moment, it is hard to quantify these effects. The formation of the Oort cloud, however, seems somewhat problematic in this picture (but see Levison et al. 2010a; Vokrouhlický et al. 2019, for a counter argument). We argue that the majority of the Oort cloud formed after the Sun escaped the cluster because perturbations of nearby stars would easily ionize an earlier Oort cloud (see also Higuchi & Kokubo 2015).

[1] For lack of better terminology, we use asteroids to indicate planetesimals or comets. A glossary of terms is available in paper I (Portegies Zwart 2021), but see also (Gladman et al. 2008).

1.2. This paper

We study the formation of the Oort cloud from a numerical perspective. The chain of events that lead to the Oort cloud can now be simulated in its entirety, although not fully self consistently. We desire to revisit this problem because we feel a bit overwhelmed by the literature's enormity and the slightly changing views over the years. We hope to contribute to a clearer picture of the processes that appear to be relevant for the formation and evolution of the Oort cloud.

We perform a numerical investigation and show that the Oort cloud was not formed in any straightforward manner, but resulted from a complicated interplay between the Sun and neighboring stars during the Sun's infancy, free-floating debris, the Galactic tidal field and planetary scattering. Each of these components turn out to be important, although their relative contributions are sometimes hard to quantify. The lack of a simple formation mechanism but a comspiracy of processes not persé make the Oort cloud unique. A complicated story requires a complicated numerical approach that covers many time and size scales. Apart from stellar evolution in the early star-cluster phase, the physics is relatively simple. We deal with the fundamentally chaotic nature of the underlying physics (see Miller 1964; Goodman et al. 1993), by repeating calculations with a different random seed. In this discussion, we limit ourselves mainly to Newtonian physics (Newton 1687). We address each component of this calculation separately but knit the results together to a homogeneous narrative on the formation and evolution of the Oort cloud as part of the Solar system.

The timescale of Oort-cloud formation is probably closely connected to the birth environment of the Solar system (Brasser et al. 2012). If born in a star cluster, as argued in Portegies Zwart (2009); Adams (2010); Parker (2020); Pfalzner & Vincke (2020), with a characteristic size of $\sim$ 1 pc and with $\sim$ 2500 siblings (Portegies Zwart 2019) asteroids in wide and highly elliptic orbits are vulnerable to being stripped from the solar system by the cluster potential or by passing stars (see also Nordlander et al. 2017). Pfalzner & Vincke (2020) however, derive an even higher density cluster with a density up to $\sim 10^5\, M_\odot/\mathrm{pc}^3$. If formed too early in the Solar-system's lifetime, the outer parts of the Oort would be lost due to stripping when a small change in relative velocity $\delta v \equiv dv/v \gtrsim \mathcal{O}(10^{-4})$ is induced upon the asteroids (see Fig. 1). So long as the Sun is a cluster member, asteroids with an eccentricity of $e \gtrsim 0.98$ with semi-major axis $a \gtrsim 2400$ au ($a(1-e) \gtrsim 50$ au) are easily lost.

In the next section we will discuss the state of affairs of our understanding of the outer solar system, followed by a description of the numerical setup and its ingredients in section 3. In section 4.1 we discuss the simulation results, and describe a holistic view on the evolution of the Sun and proto-Oort cloud in the Galaxy in section 4.2.1. The consequences of resonant planetary orbits are discussed in section 4.2.2. These arguments are supported by simulations presented in table 6. To further explore the consequences of alternative models on the formation of the Solar system, we include calculations adopting planetary orbits in resonance. We conclude in section 5.

2. State of affairs in the outer Solar system

We summarize our current understanding of the remote parts of the Solar system, starting with the Kuiper-belt region, and subsequently move on to the outer parts of the Solar system.

Four regimes in the outer part of the Solar system are important for this discussion, including: the dynamical class of trans-Neptunian objects (TNOs), the parking zone[2], the Hills cloud and the Oort cloud (for a review see Malhotra 2019). The inner three regions could have been populated and affected by encountering stars before the Sun escapes the cluster. In that case, the presence and orbital distribution of asteroids in the parking zone and Hills cloud may provide interesting constraints on the dynamical evolution of the Sun in its birth cluster before it was ejected (see also Moore et al. 2020).

2.0.1. The trans-Neptunian region and Kuiper belt

The phase-space structure in the Edgeworth-Kuiper belt is complex (Edgeworth 1943; Kuiper 1951). Close to the perturbing influence of Neptune (the red curve in figure 1 marks the outer boundary of the conveyor belt[3], see the dotted line in fig 6) we find multiple families of Kuiper-belt objects. The most striking might be the scattered disk (Brown 2001; Luu & Jewitt 2002; Trujillo et al. 2000; Nesvorný 2020), but there are other exotic orbital families observed in this region, including the warp (at an inclination of $i = 1^\circ.8^{+0^\circ.70}_{-0^\circ.4}$, Volk & Malhotra 2017), the mix of resonant families (Chiang et al. 2003), the broad distribution in eccentricity and inclination of the Plutinos (Malhotra 1993; Brown 2001), the orbital topology of the classical belt-population (Elliot et al. 2005), the outer edge at the 1:2 mean-motion resonance with Neptune (Gomes et al. 2004), and the extent of the scattered disk (Gladman et al. 2001). Except, maybe, for the population of nearly-circular objects in the classical Kuiper belt (Tegler & Romanishin 2000), many of these characteristics can be explained at least qualitatively with some incarnation of the Nice model (Gomes et al. 2005; Morbidelli et al. 2005; Tsiganis et al. 2005; Levison et al. 2008, see § 2.2 for more on the Nice model). Some of these features in the Kuiper belt originated $\gtrsim 50$ Myr after the planets formed (Nesvorný 2020).

Here we demonstrate that it is possibly to reconstruct part of the Solar system's past from the kinematics and phase-space distribution of the orbiting bodies (see also Moore et al. 2020). Although we consider the Edgeworth-Kuiper belt crucial in understanding the formation and early evolution of the Solar system, this manuscript focuses on the Oort cloud and its formation.

2.0.2. Sedna, other trans-Neptunian objects in the parking zone and the Hills cloud

So far, several asteroids have been observed beyond the Kuiper cliff (at ~ 48 au), between a few 100 au, and a few 1000 au with a pericenter distance $\gtrsim 50$ au (Sheppard et al. 2019; Alexandersen et al. 2019). These include the dwarf planet 90377 Sedna (Brown et al. 2004), 2012 VP113 (Sheppard et al. 2014) and a dozen others. They can be divided into two clusters, one population with their argument of pericenter $\sim 310^\circ$ (Trujillo & Sheppard 2014), and one population at the opposite side (Sheppard et al. 2019). This small number of known detached trans-Neptunian objects

[2] The parking zone is the region where asteroids (or dwarf planets) in orbit around the Sun are not affected by the giant planets, and also hardly affected by the Galactic tidal field or an occasional encounter with a field star (Portegies Zwart & Jílková 2015; Vargya & Sanderson 2020). It is called the *inert zone* by Saillenfest (2020) and the *forbidden region* by Correa-Otto & Calandra (2019)

[3] Area in semi-major axis and eccentricity where an asteroid crosses the orbit of one or more of the major planets, causing their orbits to drift to higher eccentricity and larger semi-major axis while preserving pericenter distance.

can, in part, be attributed to observational selection effects because they are far (Alexandersen et al. 2019), red (Brucker et al. 2009), and they tend to have a relatively small albedo (Rabinowitz et al. 2006).

Also from the outer regions of the Solar system, the area in phase space when Sedna and family is found is hard to reach, meaning that the asteroids in this region cannot have come from either direction; the inner Solar system or the periphery. This unreachable area in parameter space is called the parking zone (Jílková et al. 2015), and it is identified as such in fig. 1. Asteroids in this region keep their orbital parameters for a very long time, possibly even as long as the solar system's age. Note that, if the asteroids in the parking zone cannot have come from the inner Solar system, and they do not have an origin from the periphery, they either formed in situ or were injected there by other means. The several observed dwarf planets and asteroids (such as Sedna) in this region preserve evidence for the dynamical history of the Solar system (Kaib & Quinn 2008; Jílková et al. 2015) and can be used to constrain the the Solar system origin.

These arguments led to the possibility that Sedna and family were captured from another star in the parent cluster (Jílková et al. 2015). In this case, Sedna and family would have been captured from the circumstellar debris disk around another star. The population of asteroids in the parking zone may then form the leftover evidence for such a captured population (Nurmi et al. 2002; Morbidelli & Levison 2004; Shankman et al. 2011; Napier et al. 2021a).

Such a capture then must have happened more than $4\,\mathrm{Gyr}$ ago, and in that time frame the influence of the ice-giant planets would have caused the orbits of Sedna and family to change, in particular their arguments of pericentra should random. But their orbits are such that they pass pericenter at the same side of the Sun (Trujillo & Sheppard 2014).

Based on the alignment of the arguments of pericentra of the Sedna-family of objects, Batygin & Brown (2016) and Batygin et al. (2019) argued in favor of the existence of a planet in the inner Oort cloud. Such a planet in a wide orbit or possibly even a stellar companion to the Sun could induce orbital characteristics similar to those observed in Sedna and other detached trans-Neptunian objects (Nesvorný 2020), or and even affect the orbits of asteroids in the parking zone (Madigan & McCourt 2016; Zderic & Madigan 2020).

The main motivation for an extra planet disappeared, as the alignment of the arguments of pericentra turn out to be an observational selection effect (Sheppard et al. 2019; Napier et al. 2021b). Although a binary companion is currently probably absent (Melott & Bambach 2010; Hills 1984; Hut 1984), the Sun might have had one in the past (Siraj & Loeb 2020); in particular since such wide stellar companions are rather common among other stars (Kaib et al. 2013).

Further out, we find the hypothetical Hills cloud Hills (1981); between the outer edge of the parking zone ($\gtrsim 1\,000\,\mathrm{au}$) and the inner edge of the Oort cloud ($\lesssim 20\,000\,\mathrm{au}$). The origin of the objects in the Hills cloud is unclear, but the population could be related to trans-Neptunian objects (Fernandez & Ip 1981; Dones et al. 2015). Hills (1981) estimated the total mass to exceed the Oort cloud by as much as a factor of 100 (see however Dones et al. 2000, who argue in favor for comparable populations). The majority of trans-Neptunian objects have prograde orbits (Kavelaars et al. 2020) and isotropic distributions in mean anomaly, longitude of the ascending node, and the argument of perihelion (Bernardinelli et al. 2020). These support an inner Solar system origin because asteroids scattered from the circumstellar disk tend to have prograde orbits (Moore et al. 2020), whereas the orbits of captured asteroids may well be retrograde, depending on the encounter that introduced them in the Solar system (see also Hanse et al. 2018; Napier et al. 2021a). The dynamical history of the Solar system in its birth cluster then plays an important role in the formation and orbital topology of asteroids in the parking zone and the Hills sphere (Parker 2020). Due to the lack of perturbing influences signatures of a captured population in the parking zone remain noticeable for much longer than in other parts of the Solar system.

2.0.3. The Oort cloud

The discussion on the Öpik-Oort cloud started in 1932 by Öpik (Öpik 1932) who discussed the origin of nearby parabolic orbits in the Solar system, and in 1950 by Oort (Oort 1950) with the discovery of a spike in the reciprocal orbital separation $1/a \lesssim 10^{-4}\,\mathrm{au}^{-1}$ of observed comets. Oort (1950) argued that the long-period comets originated from a region between 25 000 au and 200 000 au from the Sun. Today, these estimates have not changed much (Correa-Otto & Calandra 2019).

The outer limit is considered to coincide with the Hill radius (Hill 1913) of the Sun in the Galactic potential (Chebotarev 1965). The inner edge's origin and precise location is less clear (Hills 1981; Leto et al. 2008) and still debated (Brasser & Schwamb 2015). It is somewhat unclear what defines the transition region between the Hills cloud and the Oort cloud.

The mass of the Oort cloud is estimated to range from $1.9\,\mathrm{M}_\oplus$ (Weissman 1996) to $38\,\mathrm{M}_\oplus$ (Weissman 1983). These estimates seem somewhat on the high side when compared to those based on numerical simulations, which arrive at $0.75 \pm 0.25\,\mathrm{M}_\oplus$ (Brasser 2008) to $1.0 \pm 0.4\mathrm{M}_\oplus$ (Fernández & Brunini 2000).

With a typical comet-mass of a few times 10^{12} to $10^{14}\,\mathrm{kg}$ (Rickman et al. 1987; Sosa & Fernández 2009, 2011) the Oort cloud contains $\mathcal{O}(10^{12})$ comet-sized objects. Interestingly, this estimate is comparable to Oort's original estimate of $\sim 10^{11}$ objects (Oort 1950), and to the density of interstellar asteroids (Engelhardt et al. 2017; Portegies Zwart et al. 2018; 'Oumuamua ISSI Team et al. 2019; Pfalzner et al. 2020).

2.1. The Formation and early evolution of the outer Solar System

Estimates on the formation timescale of the Oort cloud range from instantaneously after the formation of the Sun (Fernández 1997), synchronously with Jupiter's formation (Stevenson & Lunine 1988; Fernández & Brunini 2000; Dones et al. 2004b), after Jupiter formed and potentially migrated (Shannon et al. 2019) to slow growth over several 100 Myr (Kaib & Quinn 2008; Nordlander et al. 2017) or even Gyr timescales (Duncan et al. 1987).

Two main scenarios are popular for the formation of the Oort cloud:

- The Oort cloud formed mainly by ejecting inner Solar-system material through planet-disk interactions (Dones et al. 2000, 2004a), or
- the Oort cloud formed through two distinct processes. Local disk-asteroids are ejected into an inner region at 3000—20 000 au, while the outer region at $\gtrsim 20\,000$ au is mainly accreted from free-floating debris in the parent star cluster (Zheng et al. 1990; Valtonen et al. 1992; Brasser et al. 2006; Brasser et al. 2007; Brasser 2008; Levison et al. 2010a). Also planets could be captured in this way (Perets & Kouwenhoven 2012), possibly explaining the origin of a hypotheti-

cal exo-planet in the outer parts of the Solar system (Mustill et al. 2016).

The relatively low mass in some of the numerically derived estimates stem from the low efficiency, which ranges from ~ 1.1 percent (Leto et al. 2008; Morbidelli et al. 2009), ~ 2 percent (Correa-Otto & Calandra 2019) to ~ 4 percent (Brasser et al. 2010), at which disk material is launched into a bound Oort cloud (Paulech et al. 2010); the majority of objects are expected to escape the Solar system or hit the Sun. The giant planets could then be insufficiently efficient in explaining the currently anticipated mass of the Oort cloud (Brasser et al. 2006; Kaib & Quinn 2008; Brasser et al. 2012).

If the entire Oort cloud originates from the depletion of asteroids between Uranus and Neptune (see also Fouchard et al. 2013), this region must have been populated by 100 to $3800\,\mathrm{M_{Earth}}$ (Fouchard et al. 2014a,b). In a disk with a density profile $\rho \propto r^{-1.5}$ between 0.1 au and 45 au about half the mass is between the orbits of the ice giants. To supply the Oort cloud with sufficient material, the proto-planetary disk must then have had a mass of 200 to $7600\,\mathrm{M_\oplus}$ (or equivalently ~ 0.001 to $0.02\,M_\odot$) in comet-sized asteroids, which is consistent with other estimates (Crida 2009).

Given the inefficiency of the ice-giants to produce the Oort cloud, more than 90% could come from elsewhere; such as the circumstellar disks of other stars (Levison et al. 2010a) or free-floating debris in the parent cluster (Zheng et al. 1990; Neslušan 2000), from the capture of interstellar objects (Valtonen & Innanen 1982; Hands & Dehnen 2020; Pfalzner et al. 2021), or accretion from circumstellar disks of other stars (Fernández & Brunini 2000; Levison et al. 2010a) .

The orbits of captured asteroids could be rather distinct from those produced by scattered asteroids from the proto-planetary disk (Hands et al. 2019; Higuchi & Kokubo 2020). In the Oort cloud, both populations will be affected by the Galactic tidal field (Duncan et al. 1987; Fouchard et al. 2006b) and probably mix on a timescale of a few 100 Myr. Orbital inclinations isotropize on this timescale, and eccentricities thermalize (Fouchard et al. 2006a; Higuchi & Kokubo 2015).

Once fully developed, the Oort cloud erodes by injecting comets into the inner Solar system through Kaib-Quinn jumpers (Kaib & Quinn 2008) or by a more gradual process (sometimes referred to as *creepers*, Fouchard et al. 2014a, 2018), but also due to encounters with molecular clouds (Duncan et al. 2011) and tidal interaction with the Galaxy (Heisler & Tremaine 1986; Levison et al. 2001; Gardner et al. 2011; Torres et al. 2019). These external perturbations may be the main cause for comets launched from the Oort cloud into the inner Solar system. This process was suggested to lead to periodic showers of comets (Davis et al. 1984; Gardner et al. 2011) causing mass extinctions every ~ 29.7 million years (Raup & Sepkoski 1984; Rampino & Prokoph 2020). Such a wide companion was never found (Luhman 2014), and re-analysis of the data shows that there is no statistical significant evidence for a periodicity in these mass extinctions (Patterson & Smith 1987; Jetsu & Pelt 2000; Bailer-Jones 2009).

2.2. The Nice model

Many of the model simulations above depend on some sort of chaotic reorganization in the early Solar system. This could have happened during- or shortly after the formation of Jupiter (Li et al. 2006) up to about half a Gyr after the planets formed Neslušan et al. (2009); Leto et al. (2009). This chaotic reorganization was introduced to explain the enhanced flux of asteroids throughout the young Solar system (Morbidelli et al. 2005; Tsiganis et al. 2005; Gomes et al. 2005) that could have lead to a peak in the flux of lunar impactors (late-heavy bombardment is an often used term, Hartmann 1965, 1966; Alvarez & Muller 1984; Stöffler & Ryder 2001; Neukum et al. 2001; Ryder 2002).

Follow-up analysis indicated that the impact-period could be between 4.2 to 3.5 Gyr ago (Fritz et al. 2014; Zellner 2017; Bottke & Norman 2017), rather than a peak, making the need for a disturbance in the force in the early Solar system unnecessary. Re-analysis of the lunar impact statistics by Lineweaver (2010), indicated that a high flux of impactors is not needed to explain the lunar cratering record. This study was further supported by the re-analysis of the 267 Apollo samples on ^{40}Ar/^{39}Ar isotope ratios, demonstrating that the material on the moon arrived in a continuously decreasing flux rather than a peak (Boehnke & Harrison 2016; Boehnke & Harrison 2018).

The Nice model is successful in explaining several aspects of the Solar system, including the orbital topology of the giant planets (Morbidelli et al. 2007), Uranus' obliquity (Wong et al. 2019), Trojan asteroids (Emery et al. 2015), irregular moons (Bottke et al. 2010), some morphologies of the Kuiper belt (Morbidelli & Nesvorný 2020), and several other curious orbital choreographies (Levison et al. 2008; Shannon et al. 2019). Although, the Nice model seems to fail to explain the global structure of the Oort cloud (Fouchard et al. 2018, but see also Shannon et al. 2019, for competing arguments based on the rocky comet C/2014 S3 (PANSTARRS)), it might be hard to find a single alternative model for all the most phenomena in the Solar system. One aspect of the Nice model that may be important for explaining phenomena in the Solar system is a period in which the orbits tend to change chaotically (Thommes et al. 2008). Such a chaotic phase can be initiated by planetary resonance, as in the Nice model, induced by a passing star or by the last phase of evaporation of the circumstellar disk.

Several rather independently developed explanations exist, including models based on internal dynamical processes (Duncan et al. 1995; Ida et al. 2000), encounters with other stars (Ida et al. 2000; Kobayashi et al. 2005; Torres et al. 2019) or a small molecular cloudlet in a wide orbit around the Sun (Emel'yanenko 2020). But there is no global model that explains the Solar system in unison.

This early phase in the solar system's evolution appears far from being understood from first principles, and more research on this topic would help to understand the current apparent stability and seemingly inertness of the current Solar system.

3. Methods, models and Simulations

This section explains the numerical methods, the initial conditions, and simulations used to qualify and quantify the formation and early evolution of the Oort cloud. Our calculations are not self-consistent because the results were not produced in a single simulation, but the results are melded together to form a consistent understanding.

We start with a discussion on the software framework, the Astrophysics Multipurpose Software Environment (or `AMUSE`, see section 3.1), which was used for the simulations presented here. We discuss each of the following processes:

A The evolution of the circumstellar disk of an isolated Solar system (see section 3.2, and table 1).
The calculation includes the 4 giant planets orbiting the Sun together with a disk of mass-less particles. The entire setting

Scattered and captured asteroids (see sect. 3.2)	
Designation	Simulation A.
Simulations	2 simulations of the Solar system with planets, scattered and captured asteroids in the Milky way potential.
Star	Single 1 $M_\odot$ star in the smooth potential of the Milky Way Galaxy.
Planets	4 planets per star in a circular disk, with Jupiter, Saturn, Uranus and Neptune in circular orbits with semi-major axis of 5.1, 9.5, 19.2, 30.1 au.
Asteroids	One simulation with 2000 asteroids (from planetary system # 157 of sect. 3.3.2 (see also Torres et al. 2020a). One simulation with 1888 asteroids (from the most probable encounter that, according to Jílková et al. (2015) resulted in a population of Sedna-like objects.
Numerics	`Huayno` (Pelupessy et al. 2012) coupled with the Galactic model (see table 4) via bridge (Portegies Zwart et al. 2020) in `AMUSE` (Portegies Zwart & McMillan 2018).
Computer	run on Cartesius, and ALICE using GPU.
Duration	The simulations started at an age of $\sim$ 100 Myr. By that time, the solar system has left the parent cluster, and continue for 1 Gyr.

Table 1. Simulations of the Solar system with captured and scattered asteroids in the Galactic potential.

Star cluster simulation (see sect. 3.3)	
Designation	Simulation B.
Simulations	200 simulations with 200 asteroids per star, and 24 simulations with 2000 asteroids per star in a cluster where stars interact with the asteroids.
Stars	2000 stars with a Kroupa (2001) mass function between 0.08 and 100 $M_\odot$in R=1pc virialized Plummer sphere (Plummer 1911). No primordial binaries, no residual gas.
Planets	4 planets per star with circular orbits. Each star has the same planetary systems in a plane, but each planetary system has a different random orientation in space. In one model (extended) the planets Jupiter, Saturn, Uranus and Neptune have an initial semi-major axis of 5.1, 9.5, 19.2, 30.1 au. In the other model (compact), Jupiter, Saturn, Neptune and Uranus have an initial semi-major axis of 5.5, 8.1, 11.5, 14.2 au.
Asteroids	in a disk between 40 au and 1000 au in the extended model and between 16 au and 400 au in the compact model
Numerics	`NBODY6++GPU` (Wang et al. 2015) and `REBOUND` using IAS15 integrator (Rein & Spiegel 2015) coupled via the LonelyPlanets scheme (Cai et al. 2019) in `AMUSE` (Portegies Zwart & McMillan 2018).
Computer	run on GPU-equipped Little-Green-Machine-II (LGM-II) computer.
Duration	The simulations start with all stars on the zero-age main-sequence with 4 planets in the adopted initial orbits. The calculation is continued for 100 Myr.

Table 2. Simulations performed of the Solar system in its birth star cluster using the *LonelyPlanets* approach (see sect. 3.3.1). The resulting orbital distribution of asteroids from the Sun-representative star is used in this work to explore further the evolution of the distribution of asteroids in the Oort cloud. These simulations do not lead to a reliable representation of abducted asteroids, because the lonely planet approach does not allow exchange interactions.

is integrated in the potential of the Galaxy, starting with the approximate position in the Galaxy where the Sun was 1 Gyr ago, and lasted for a Gyr.

B The evolution of the Solar system in its birth cluster (section 3.3, and table 2).
The arguments here are based on two quite distinct calculations, first a simulation of 2000 stars in a virialized cluster with a half-mass radius of $\sim$ 1 pc. We study the evolution of debris disks under the influence of the encounters with neighboring stars. In a second calculation, we study the exchange-efficiency and orbital characteristics of the circumstellar disks that got perturbed in encounters between two stars. These two simulations are used to understand the orbital parameters of various populations of asteroids:
   1. The captured asteroids and their migration towards the Oort cloud (see section 3.3.2),
   2. and the scattered-disk asteroids along the conveyor belt (see section 3.3.3).

C Transport of asteroids along the conveyor belt and eccentricity damping by the tidal field once the Oort cloud is reached (see section 3.4, and table 3).

The formation of the Oort cloud is supported by simulations on the population of asteroids in the conveyor-belt region. These calculations include the 4 giant planets (with various orbital configurations) and the Galaxy's tidal field. Both are necessary to study the transport of asteroids from the planetary region to the Oort cloud. The eccentricity and semi-major axis of the asteroids increases when evolving along the conveyor belt. This process is driven by the major planets. Once the pericenter of the asteroid's orbits detaches from the major planets, the Galactic tidal field dampens the eccentricity of the orbits.

In fig. 1, we present a schematic overview of the evolution of the Oort cloud. Asteroids near Jupiter and Saturn are vulnerable to being ejected on a relatively short timescale ($\lesssim$ 10 Myr), whereas asteroids originally formed between Uranus and Neptune, and the scattered and captured populations (green arrows), tend to reach the Oort cloud on a much longer timescale of $\sim$ 100 Myr. All asteroids that eventually reach the Oort cloud pass through the narrow neck at eccentricity $\gtrsim 0.998$ at a semi-major axis around 10^4 au after which they are subjected to ec-

centricity damping by interacting with the Galactic tidal field (green arrows to the right in fig. 1). In figure 2, we present a superposition of simulation data ~ 100 Myr after the Solar system escaped its birth star cluster. This data originates from multiple calculations that simulate various aspects of the formation of the Oort cloud.

3.1. The Astrophysics Multipurpose Software Environment

The calculations in this study are performed using the Astrophysics Multipurpose Software Environment (Portegies Zwart & McMillan 2018). `AMUSE` is a modular language-independent framework for homogeneously interconnecting a wide variety of astrophysical simulation codes. It is built on public community codes that solve gravitational dynamics, hydrodynamics, stellar evolution, and radiative transport using scripts that do not require recompilation. The framework adopts *Noah's Arc* philosophy, meaning that it has incorporated at least two codes that solve the same physics (Portegies Zwart et al. 2009).

Most calculations are carried out using a combination of symplectic direct N-body, test-particle integration and the tidal field of the Galaxy. For the former two, we use `Huayno`, which adopts the recursive Hamiltonian splitting strategy (much like bridge, see Fujii et al. 2007; Portegies Zwart et al. 2020) to generate a symplectic integrator that conserves momentum to machine precision (down to 10^{-14} in normalized units, Pelupessy et al. 2012). Additional calculations were performed using the ABIE code (Cai 2018), `NBODY6++GPU` (Wang et al. 2015) and `REBOUND` (Rein & Liu 2012) using IAS15 scheme (Rein & Spiegel 2015). These methods are combined using the `AMUSE` framework in the LonelyPlanets approach (Cai et al. 2019, see also section 3.3.1).

Where appropriate, we include stellar mass loss in our calculations using the `SeBa` binary population synthesis package (Portegies Zwart & Verbunt 1996; Toonen et al. 2016). For the Galaxy, we take a slowly varying potential of the bar, bulge, spiral arms, disk, and halo into account. The parameters for the Galaxy model are listed in table 4 (see also Martínez-Barbosa et al. 2015, 2016, 2017).

The galactic tidal-field code is coupled to the various N-body codes using the augmented non-linear response propagation-pattern (called *rotating bridge* in Martínez-Barbosa et al. 2017). The interaction time-step between the Galactic tidal field and the Solar system was 100 yr. This time step suffices because the period of the asteroids in such wide orbits exceed 0.1 Myr.

3.2. Evolution of the circumstellar disk of an isolated Solar system

The simulations presented in this section aim to understand the consequences of evolution of the newly born Solar system with a disk of planets and asteroids as part of the Galactic tidal field. The Solar system is initialized in the Galactic potential at -8.4 kpc along the x-axis and 17 pc above the Galactic plane. The initial velocity of the Solar system was $v_\odot = (11.352, 233.105, 7.41)$ km/s, which follows an almost circular orbit around the Galactic center (see figure 3). From this position and velocity we calculate the Sun's position in the Galaxy backwards for 1 Gyr, which is where our calculations start. The location of the Solar system 1 Gyr ago then was $(-4.451, 7.796, 53.99)$ kpc, with a velocity of $(204.1, 101.3, 5.742)$ km/s.

We initialized the Solar system with the four giant planets, Jupiter, Saturn, Uranus, and Neptune, as they appear in their orbit on 1 January 2020 (2020-01-01T00:00:00.000 UTC), according to the JPL Horizon database[4] (Bear in mind here that the choice of the initial Epoch should not matter much for either the qualitative or the quantitative statistical results. For the orbits of individual asteroids, the precise initial realization is important, though, see section 4.4.2 for a brief discussion). The ecliptic was initialized with an angle of 60° to the Galactic plane. The initial conditions for these simulations are presented in table 1. A wider range of initial realizations was tried, including changing the orbital phases, and separations of the planets and the parameters for the debris disk (see section 4.1). Varying the orbital phases do not result in qualitative differences, but the results are quite sensitive to changes in the planets' initial orbital separations. After initializing the planets, we place a disk of test particles in the ecliptic plane around the Sun. The disk was generated using the routine `ProtoPlanetaryDisk` in the `AMUSE` framework with a Toomre-Q parameter of 25 (Toomre 1964). Most simulations are performed with disks, between 16 au and 35 au, but other ranges were explored with a minimum of 3 au and an upper limit of 1000 au.

In the simulations, Jupiter starts to populate the resonance regions (such as the Hilda-family of asteroids, see also the purple arrows to the bottom left in figure 1 on how they migrate) and launches asteroids into the conveyor belt (light green and black curves) directly from the start of the simulation. This process happens very early after the formation of the Solar system which may then still be a cluster member. After 1 Myr 43.4% of the asteroids born between 3 and 15 au are still in resonant orbits, and $39.4\,\%$ have escaped the Solar system (see also Pirani et al. 2018, 2019). Asteroids initially on wider orbits are not affected much in this short time frame. In figure 4 we illustrate this process by plotting the orbit of a test particle integrated with the Solar system and the tidal field of the Galaxy.

On a longer timescale, based on the simulations listed in table 3 and table 6, the ice-giant planets transport asteroids along the conveyor belt into the Oort cloud, where they slowly circularize and isotropize. After $\sim$ 100 Myr the orbital distribution of asteroids is not much different that today's; the stable resonant regions near the giant planets are populated, and the non-resonant orbits as well as the conveyor belt are depleted. Only $1.4\,\%$ of the asteroids born between 15 and 50 au is still in the disk after 100 Myr and 59.2% has become unbound from the Solar system. The remainder of the asteroids born between 15 and 50 au, has migrated to the Oort cloud.

The giant planets scatter the asteroids in inclination only by a few degrees (see also Di Sisto & Rossignoli 2020). By the time the asteroids reach the inner Oort cloud, their inclinations are still not much larger than a few 10° around the ecliptic plane. Even asteroids that are scattered along the conveyor belt to the Oort cloud preserve a relatively low inclination with respect to the ecliptic plane (see also Duncan et al. 1987; Correa-Otto & Calandra 2019). The inclination distribution only isotropizes once the Galactic tidal field starts to dominate the asteroids' orbital evolution(see also Fouchard et al. 2018). Although the majority of asteroids escape the Solar system while being kicked out by the planets, the number that remain bound is sufficient to explain the richness of the predicted population of objects in the Oort cloud.

The schematic view presented above, however, is rather idealized because we assumed that the Solar system was born as a

[4] see `https://ssd.jpl.nasa.gov/?horizons_doc`

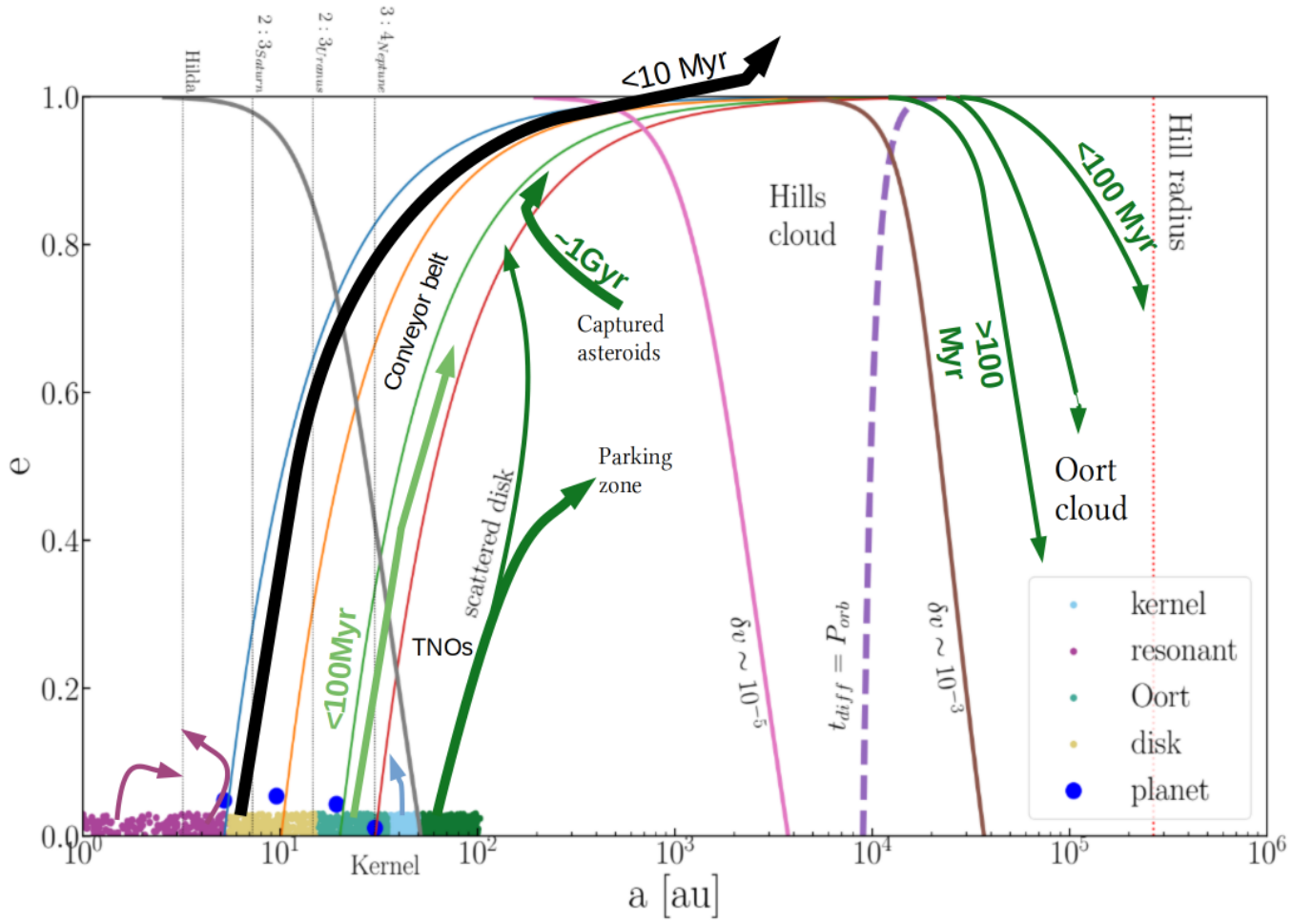

Fig. 1. Orbital migration of asteroids and how they end-up in the Oort cloud. Several of the thin curves are also plotted in fig. 2. The 4 major planets are indicated with their current semi-major axis and eccentricity as blue dots. The initial circumstellar disk is presented in five colors, depending on their final destination of the asteroids populating the different disk sections. The arrows indicate the movement of asteroids originating from the disk or captured from other stars. The timescales presented near the arrows give an estimate of the timescale of migration. The colors indicated in the legend give the original inner disk (magenta), which mainly migrate away from resonant orbits (Delbo' et al. 2017) (4 important resonances are indicated with thin vertical dotted lines). Ogre indicates those asteroids that are ejected from the Solar system on a relatively short timescale ($\lesssim 10$ Myr). Light blue indicates the kernel and the resonant Kuiper belt. The light green and dark green curves show the asteroids' migration patterns that eventually reach the Oort cloud. These objects migrate from a semi-major-axis of a few 10 au to beyond 10^4 au through a narrow neck of high eccentricity. The asteroids in the dark green area require external support from a stellar encounter to be able to migrate to the Oort cloud. This migration is better visible in fig. 2, where the eccentricity (y-axis) is in logarithmic units. Note that the closer an asteroid is to the Hill radius (vertical red-dotted line to the right), the quicker its orbit will be circularized by the Galactic tidal field (see also fig. 7, where this is illustrated). The gray, pink and brown curves indicate where the relative velocity kick imparted at apocenter by the Galactic tidal field to an asteroid is $\delta v = 10^{-8}$, 10^{-5} and 10^{-3} of the orbital velocity, respectively. The purple dashed curve indicates the orbital separation and eccentricity for which the tidal eccentricity damping timescale equals the orbital period (see Duncan et al. 1987).

single star orbiting in the Galactic potential. In the following section we will relax this assumption and study the consequence of the Sun being born in a young stellar cluster. It turns out that being born in a clustered environment has profound consequences for the efficiency on the formation of the Oort cloud.

3.3. The evolution of the Solar system in its birth cluster

For the simulations presented in this section, the Solar system is initialized as a member of a star cluster (see also Torres et al. 2020a; Stock et al. 2020; Veras et al. 2020). Two series of simulations were performed: one in which the Sun has four giant planets in a compact configuration, and the other that shows a more extended configuration (see table 2). Simulations are performed with 2000 asteroids in circular orbits between 16 au, and 35 au for the compact, and another series with asteroids between 40 and 1000 au for the extended configuration (see also Torres et al. 2020a). An additional set of 32 simulations (not listed in table 2) was performed in which the Solar system with a disk of 1000 asteroids experiences a single close encounter at a distance of 225 au or 400 au with a relative velocity of 1 km/s. Here we varied the impact angle of the encountering star from 0° (in the ecliptic plane), 30° 60° and 90° (perpendicular to the ecliptic).

In these models, we ignore the inner disk (within 40 au for the extended models and within 16 au for the compact models). This is motivated by the fragility of the inner solar system. Any encounter that would perturb the inner region probably leave the Solar system unrecognizable today. Therefore, there seems to be no particular reason to include the inner disk in the calculations. Each simulation was performed up to 100 Myr. This time scale

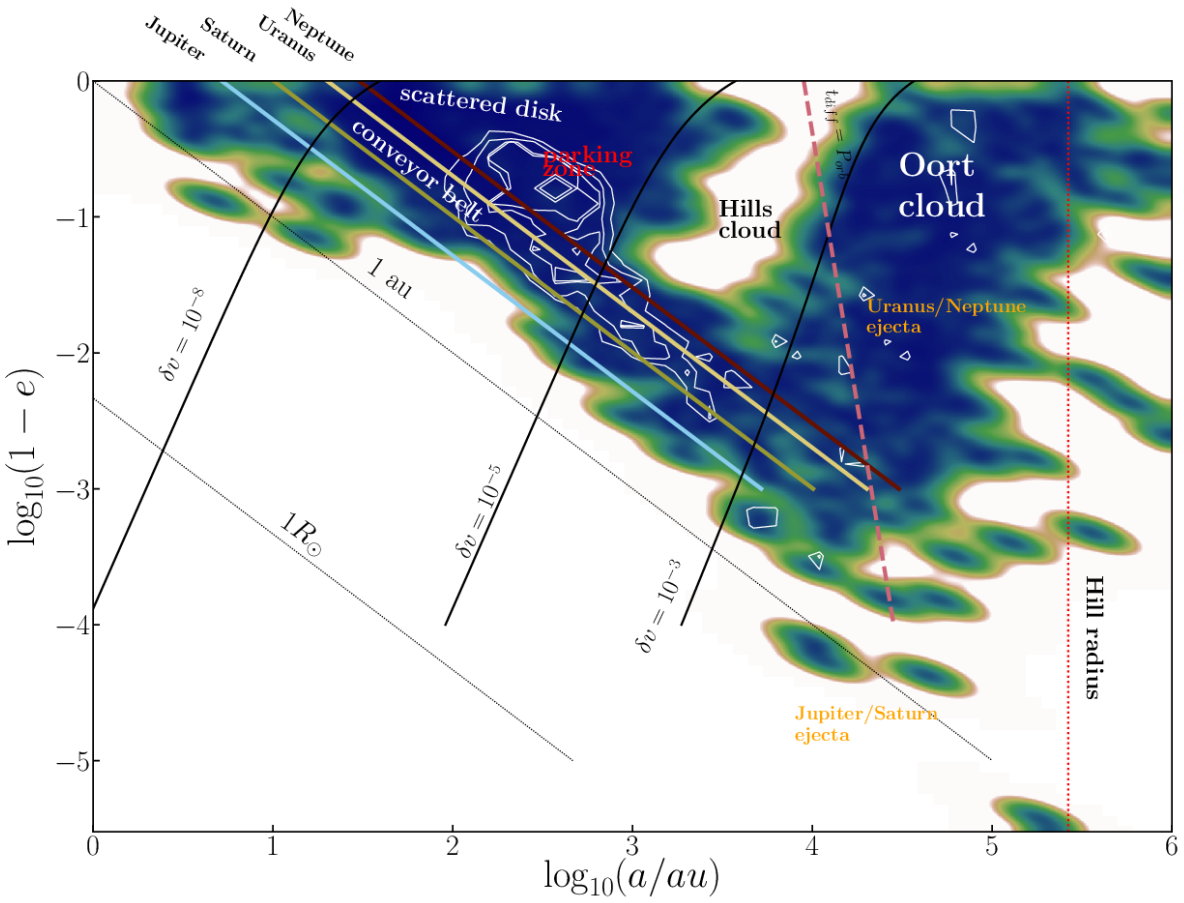

Fig. 2. Phase-space distribution of asteroids around the Sun $\sim$ 100 Myr after escape from its parent cluster. The shaded region presents a kernel-density estimation of the simulation results, representing various families of objects. We adopted non-parametric Gaussian kernel density estimator with a symmetric bandwidth of 0.02 (Scott 1992). At this moment, part of the Oort cloud is already in place (to the right), but the formation process is still ongoing. The colored diagonal curves (from top left to bottom right) indicate orbits that cross the giant planets' (see also fig. 1). The dashed burgundy-colored curve to the right indicates where the orbital period, $P_{\rm orb}$, equals the eccentricity damping-diffusion timescale by the Galactic tidal field ($t_{\rm diff}$, Eq.5 of Duncan et al. 1987). The solid black curves indicate the Galaxy's perturbing influence in terms of the velocity-kick imparted to an object. Relative velocity perturbations of $\delta v = 10^{-3}$ (right), 10^{-5}, 10^{-8} (left) are indicated. The little area to the right of Neptune's influence (between the red diagonal curve and the black curve indicating a perturbation $\delta v = 10^{-8}$) corresponds to the Kuiper-belt kernel distribution. The parking zone is indicated in red. The Oort cloud is to the right of the rightmost solid black curve (labeled as $\delta v = 10^{-3}$) and the burgundy-colored dashed curve. The Hills cloud is to the left of this dividing line (indicated in black). In our simulations the Hills cloud at low eccentricity ($e \lesssim 0.95$) is mostly empty, but at higher eccentricity (near the bottom of the figure) it's population is substantial, in particular along the conveyor belt. The captured and scattered asteroids are indicated in white contours. Locally at the extreme, both populations have comparable phase-space density. At the age of 100 Myr, a considerable fraction of the native disk population already made it to the Oort cloud, or are on their way to it through the conveyor belt. Some captured asteroids are currently migrating along the conveyor belt and a few already made it to the Oort cloud. The majority of the scattered and captured asteroids, however, is in the parking zone between $\sim$ 100 au and $\sim$ 1000 au, where they will stay for the duration of the simulation. Jupiter and Saturn eject asteroids along the conveyor belt into escaping orbits (indicated in orange). Uranus and Neptune eject asteroids on a timescale considerably longer ($\gtrsim$ 100 Myr) than Jupiter and Saturn ($\lesssim$ 10 Myr), allowing these asteroids to be circularized by the Galactic tidal field (also in orange). This is also visible in the lower kernel-density along the Jupiter-Saturn conveyor belt in comparison with the Uranus-Neptune conveyor belt. Eventually, the latter asteroids become the members of the Oort cloud. The red-dotted curve indicates the Hill radius of the Sun in orbit around the Galactic center, here at about 0.65 pc. The thin dotted diagonal curves indicate pericenter distances of 1 au and 1 $R_\odot$. Comets from the Oort cloud may enter the inner Solar system (to the far bottom right and below the 1 au curve).

is smaller than the cluster lifetime, but it suffices to support the conclusions of this paper.

The cluster in those simulations are performed using `NBODY6++GPU` (Wang et al. 2015), while we use `REBOUND` (Rein & Liu 2012) for integrating the planetesimals (using the IAS15 integration scheme from Rein & Spiegel 2015). The simulations are carried out using the LonelyPlanets approach designed in Cai et al. (2017, 2018, 2019).

3.3.1. Simulating planetary systems in a dense star cluster: the LonelyPlanets approach

In the LonelyPlanets module in `AMUSE` we first evolve a star cluster without planets or asteroids for 100 Myr using NBODY6++GPU (Wang et al. 2015). This calculation includes the N-body dynamics of the stars, stellar evolution and the interaction with the Galactic tidal field (as described above). Clusters are born instantaneously without residual gas and with stars

Simulation of the migration of asteroids from the conveyor belt to the Oort cloud (see sect. 3.4).	
Designation	Simulation C.
simulations	9 simulations with various initial realizations, but geared toward populating the Oort cloud from the conveyor belt.
Planets	4 planets to each star in a circular disk. with Jupiter, Saturn, Uranus and Neptune in orbits with semi-major axis of 5.1, 9.5, 19.2, 30.1 au.
Asteroids	10^4 asteroids per run distributed in the ecliptic plane in the conveyor belt on eccentric orbits between 0.1 and 0.9 and with peri-center distance between 5.1 au and 30.1 au (see also Duncan et al. 1987). 4 simulations with the ecliptic plane in the Galactic plane and 5 simulations with an inclination of 60° to the Galactic plane.
Numerics	`Huayno` (Pelupessy et al. 2012) coupled with the Galactic model (see table 4) via bridge (Portegies Zwart et al. 2020) in `AMUSE` (Portegies Zwart & McMillan 2018). 7 simulations were conducted with standard precision of the `Huayno` integrator, and two simulations at twice the precision (by reducing the time-step parameter η from 0.02 to 0.01).
Computer	run on ALICE using GPU.
Duration	start at an age of $\sim$ 100 Myr (once the solar system left its birth cluster, and continued for 1 Gyr ($\sim$ 1 Gyr after the Sun left the cluster, see sect. 3.3.4).

Table 3. Simulation of the Solar system with asteroids in the conveyor belt. These simulations are performed with a populated conveyor belt. The initial conditions for the asteroids are therefore not the result of earlier calculations. These conditions were selected to mimic the phase in which asteroids are launched onto the conveyor belt. Since this process may last for up to some 100 Myr, we short-tracked this by generating initial conditions when the asteroids are already in the conveyor-belt region. These simulations are mainly used to study the Galactic tidal field's eccentricity-damping process and the phase-space distribution of asteroids in the Oort cloud.

Table 4. Model parameters of the Milky Way.

Axisymmetric component		
Mass of the bulge ($M_{\rm b}$)	1.4×10^{10} M$_\odot$	
Scale length bulge (b_1)	0.3873 kpc	
Disk mass ($M_{\rm d}$)	8.56×10^{10} M$_\odot$	
Scale length 1 disk (a_2)	5.31 kpc	1)
Scale length 2 disk (b_2)	0.25 kpc	
Halo mass ($M_{\rm h}$)	1.07×10^{11} M$_\odot$	
Scale length halo (a_3)	12 kpc	
Central Bar		
Pattern speed ($\Omega_{\rm bar}$)	40 km s^{-1} kpc^{-1}	2)
Mass ($M_{\rm bar}$)	9.8×10^9 M$_\odot$	4)
Semi-major axis (a)	3.1 kpc	5)
Axis ratio (b/a)	0.37	5)
Vertical axis (c)	1 kpc	6)
Present-day orientation	20°	3)
Spiral arms		
Pattern speed ($\Omega_{\rm sp}$)	20 km s^{-1} kpc^{-1}	2)
Number of spiral arms (m)	2	7)
Amplitude ($A_{\rm sp}$)	3.9×10^7 M$_\odot$ kpc^{-3}	4)
Pitch angle (i)	15.5°	4)
Scale length (R_Σ)	2.6 kpc	7)
Scale height (H)	0.3 kpc	7)
Present-day orientation	20°	5)

References: 1) Allen (1973); 2) Gerhard (2011); 3) Romero-Gómez et al. (2011); 4) Jílková et al. (2012); 5) Martínez-Barbosa et al. (2015); 6) Monari et al. (2014); 7) Drimmel (2000); 8) Jurić et al. (2008)

from a mass function on the zero-age main-sequence distributed in a virialized Plummer sphere. We store masses, positions and velocities on the 5 nearest neighbors for each star during the calculation at 1000-year time intervals. Interactions with a single nearest star provided satisfactory statistics for the strongest encounters (Glaser et al. 2020), but in our opinion lagged in weaker perturbations. We therefore include the nearest 5 stars.

In the second pass through the data, each stored encounter is treated as a scattering experiment lasting 1000 years. After each scattering experiment with 5 perturbing single stars and one star with planets, we continue with the new set of 5 perturning stars while carrying the planetary system over from one scattering experiment to the next, 1000 years later. This works as follows: The masses, positions and velocities of the 5 perturbing stars are recovered from file, and the target star with planets and test particles as asteroids is integrated together with the perturbers (see table 2). After 1000 years of integration, we recover the next set of 5 perturbers from file and integrate them as a new experiment together with the target star, planets and asteroids. Note that these 5 nearest neighbors may be different stars from one snapshot to the next (1000-years later). The presence of planets in the scatter experiment lead to small perturbations on the encountering stars and therefore affect their orbits. Therefore, even if a subset of perturbing stars is identical from one snapshot to the next, the positions and velocities of these perturbers does not necessarily have to be identical at the end of a scatter experiment and the beginning of the next snapshot because the encounter data-base was built without planets. Our approach, therefore, is inconsistent.

The encounter between the five perturbing stars and the one star with planets and asteroids, is calculated using `REBOUND` (Rein & Liu 2012). This process is repeated for each encounter for the duration of the star-cluster simulation (100 Myr). In Fig. 5 we present an illustration of this method with the six interacting stars identified.

In the following two sections, we discuss two populations; the captured and the scattered populations of asteroids. The amount of mass (or the number of asteroids) that is transferred is similar to the number of asteroids at the disk's periphery, which is unbound or scattered into highly eccentric and inclined orbits (Jílková et al. 2015).

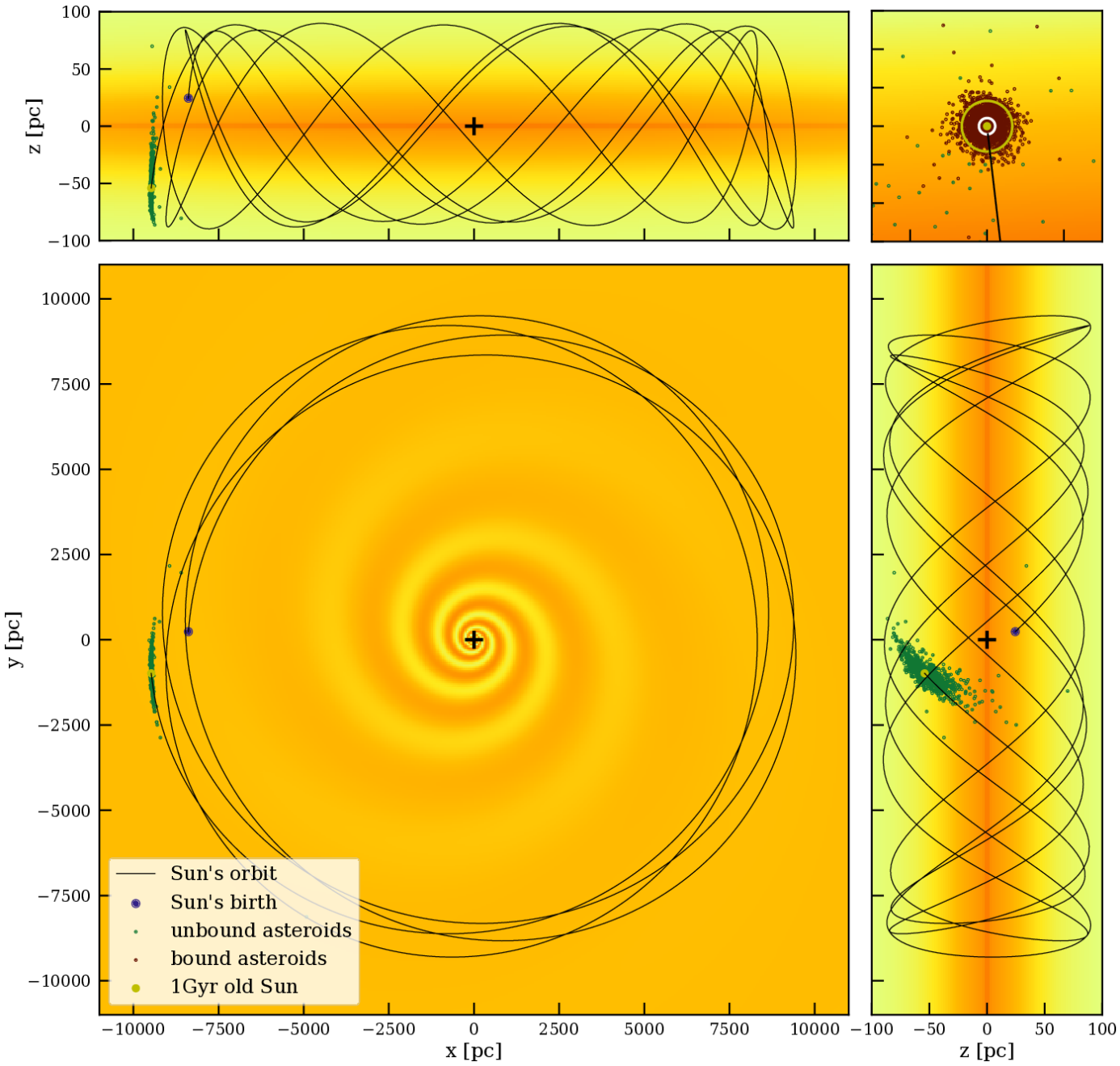

Fig. 3. Galactic distribution of asteroids 1 Gyr after the Sun escaped its birth cluster (still ~ 3.6 Gyr in the past). The colored background represents the adopted Galaxy potential: bottom left, top left, and bottom right views show the various Cartesian coordinates (the bar is not shown). The red and green dots show the bound and unbound asteroids. The Sun's starting position is also indicated. The top-right corner-panel shows a magnified view of 6 by 6 parsec around the Sun. The outer circle shows the Hill radius at ~ 0.65 pc, the inner circle represents the inner edge of the Oort cloud at about ~ 0.21 pc (at $\delta v = 10^{-3}$).

3.3.2. The influence of the cluster on the circumstellar disk

When a star is a young cluster member mutually affect the circumstellar disks (Vincke et al. 2015; Vincke & Pfalzner 2016). Most simulation studies, however address the effect of one star on the disk of another star resulting in the deformation of the disks (Breslau et al. 2014; Rawiraswattana et al. 2016; Xiang-Gruess 2016; Breslau et al. 2017). A star in a cluster is exposed to multiple encounters, each having a subsequent effect on the disk's morphology and mass. Only a few studies take these multiple interactions into account (Jiménez-Torres 2020; Torres et al. 2020a).

But mutual interactions also lead to the transport of material from one star to another (see also Korycansky & Papaloizou 1995). We address both processes separately. Here we describe the scattering of the native disk due to stellar encounters. In sect. 3.3.3, we discuss the abducted asteroids from another star's disk.

In the calculations with LonelyPlanets, we follow the dynamical evolution of the debris disk and planets around each star individually (see previous paragraph). The disks are only resolved in the second pass through the data. As a result, disks

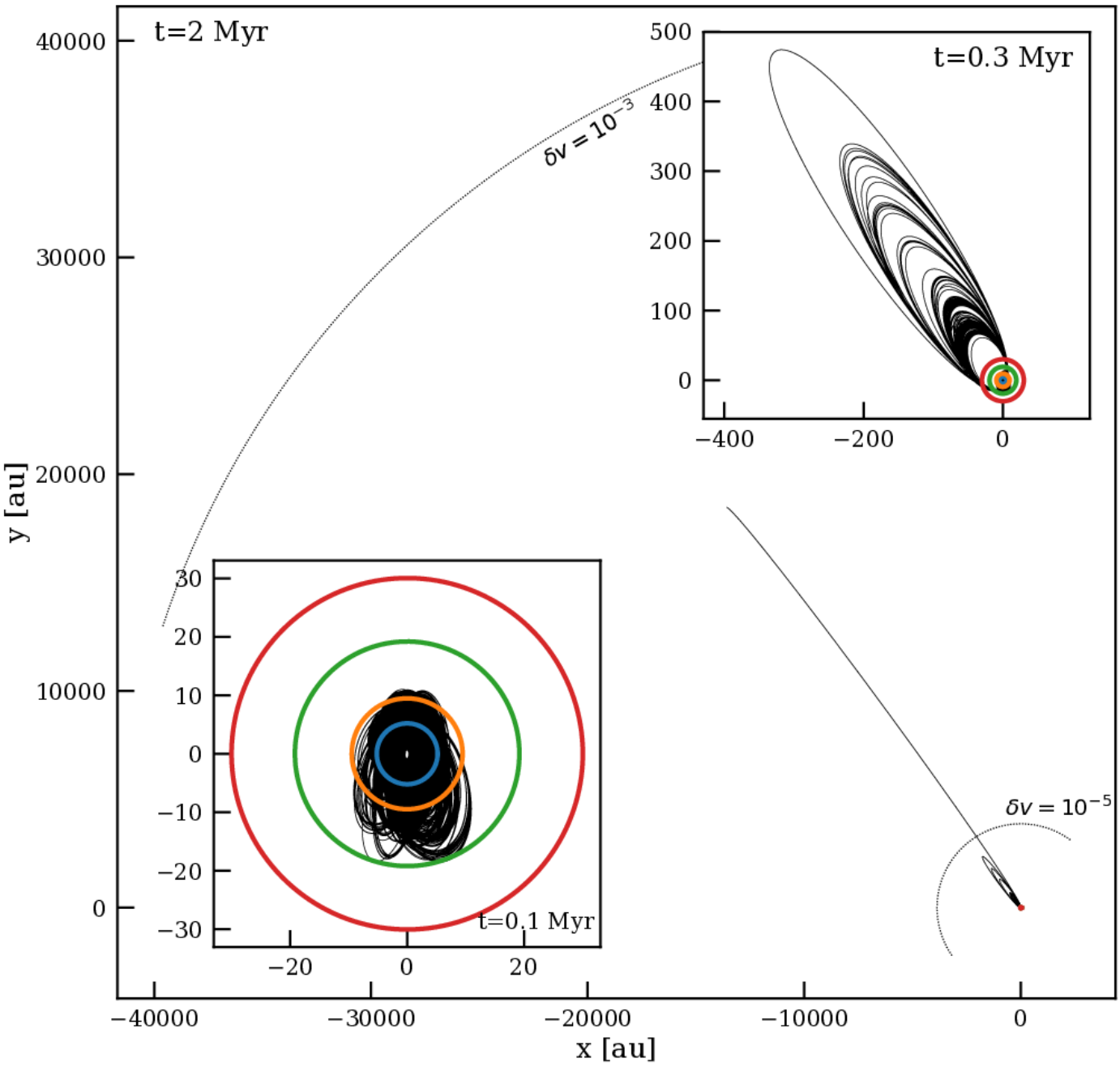

Fig. 4. First 2 Myr of orbital evolution of an asteroid, born in a circular orbit in 4:5 mean-motion resonance with Jupiter. Repeated interactions with the giant planets (colored circles: blue, orange, green and red for Jupiter, Saturn, Uranus and Neptune, respectively) launched it along the conveyor belt into the Oort cloud until it reaches the Hill sphere at a semi-major axis $\gtrsim 14\,000$ au with eccentricity $\gtrsim 0.995$. The inset to the lower left gives the first 0.1 Myr of evolution, and the inset to the top right gives the first 0.3 Myr. Each frame is on a different scale.

do not interact mutually, but they are affected by multiple encounters with other stars.

Each star experiences multiple interactions with other stars. We focus on one particular star in this simulation: the 1 $M_\odot$ star # 157 from Torres et al. (2020, their figure 2). We picked this star because the orbital topology of its scattered population resembles the Solar system's Kuiper belt. The initial inner edge of the disk in this calculation is 40 au. This seems rather large, but a strong perturbation of the more inner region, would have had considerable repercussions for the entire planetary system, contrary to what is observed in the Solar system.

In Fig. 6, we present the orbital distribution of the scattered disk population (green dots). The small black lines from each dot points in the direction of the evolution of its orbit over the next 300 Myr. The population near the inner part of the disk ($a \lesssim 50$ au) is affected by the outer planets, causing an increase in their eccentricity. The population between 50 and 500 au, is hardly affected by either the planets or by the other stars, and is hardly affected over the lifetime of the Solar system, until the Sun evolves off the main sequence and sheds its outer layers (this process was studied extensively by Veras et al. 2011; Veras & Tout 2012; Veras et al. 2014; Zink et al. 2020).

Once the star and surviving disk leave the parent cluster, $\sim 4.2\,\%$ of its native outer-disk asteroids have been scattered through interactions with other stars directly into the conveyor belt region. The majority of these asteroids move on a timescale

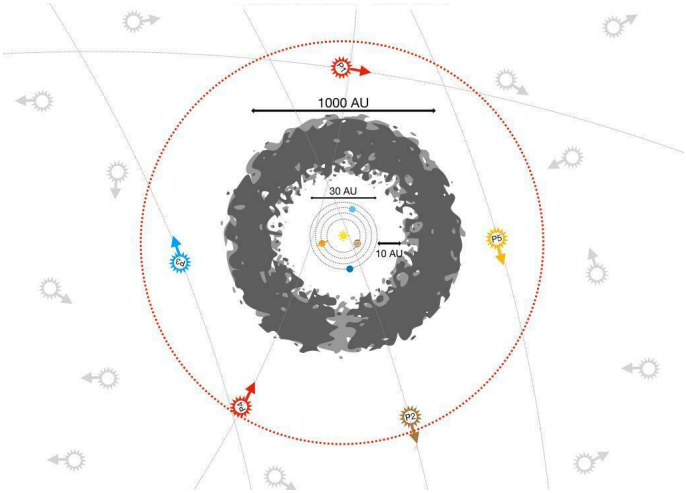

Fig. 5. Illustration of the extended Solar-system model (not to scale). The gray shaded region represents the debris disk with an outer radius of 1000 au. The dotted red circle indicates the neighbor sphere's boundary, beyond which we ignore the influence of perturbations by passing stars. Grey symbols represent the stars in the cluster that are ignored. The colored star symbols (P1, P2, P3, P4, and P5) represent the five nearest stars that perturb the solar system at a given time. The arrows indicate the direction of motion of the perturbers (figure from Torres et al. 2020a).

of ~ 100 Myr along the conveyor belt until they reach the Oort cloud (once they cross the curve $t_{\rm diff} = P_{\rm orb}$, or the curve of $\delta v = 10^{-3}$). This process is illustrated in Fig. 6 with the long lines that start at the asteroids pointing to their orbital parameters 300 Myr later in time (in the direction of the Oort cloud). Note that in Fig. 6 the curve for $\delta v = 10^{-5}$ is given, which roughly corresponds to the inner edge of the Hills cloud. The difference between the $\delta v = 10^{-5}$ and $\delta v = 10^{-3}$ is also illustrated in fig. 1 and fig. 4.

After ~ 100 Myr, some asteroids $\gtrsim 2.5$ Neptune-Hill radii from Neptune's orbit are still in the process of ascending the conveyor belt (see the thin dotted curve to the right of the red curve in figure 6). This small population of asteroids within the conveyor belt does not migrate to the Oort cloud. Di Sisto & Rossignoli (2020) found a similar population of lingering asteroids, and the migration process in their calculations takes ~ 68 Myr, which is comparable to the ~ 100 Myr in the calculations presented here. Also Fernández et al. (2004) studied the migration rate of scattered trans-Neptunian objects to the Oort cloud and argue that eventually, after 5 Gyr, half the scattered disk settles in the Oort cloud.

3.3.3. The captured asteroids

Apart from scattering the circumstellar disk, stellar encounters also lead to the capture of asteroids. The majority is deposited in the parking zone, possibly in highly inclined orbits (Jílková et al. 2016). Those that enter the conveyor belt migrate towards the Oort cloud, or are ejected. The fraction of captured asteroids that enter the conveyor belt depends on the details of the encounter, and the encountering star's disk parameters. Although the numbers vary strongly depending on the encounter parameters, the typical fraction of captured asteroids is comparable to the fraction of asteroids lost, at least in an equal-mass encounter (see also Breslau et al. 2017). Encounters in which the encountering star meets the prograde orbiting debris discs are most effective in producing unbound asteroids (Pfalzner et al. 2021). The population of captured asteroids may then have a high proportion of retrograde orbits compared to those ejected from the inner Solar system.

We included a population of captured asteroids in our analysis. The calculations using the LonelyPlanets approach, however, are not suitable for acquiring a census of their orbital distributions (Cai et al. 2018) because once an asteroid becomes unbound from its parent star it is lost from the simulation. Instead of taking the results of system # 157 from Torres et al. (2020a), as we did for the scattered disk, we adopt the results of Jílková et al. (2015) for the captured asteroids. They performed N-body calculations to study the mutual stellar encounter that could explain the orbit of the dwarf planet Sedna through the capturing from the circumstellar disk of another star in the parent cluster. The captured population from Jílková et al. (2015) reproduces Sedna's orbit as a captured object.

At the moment, Sedna orbits in the parking zone well outside the conveyor belt and it is not expected to reach the Oort cloud. From a Galactic point of view, Sedna is relatively close to the Solar system. Asteroids within $\lesssim 1000$ au to the parent star are hardly affected by the tidal field of the Galaxy. The parking zone is then composed of a roughly equal number of scattered and captured asteroids, and their orbits are expected to be hardly affected by either the planets or by the Galactic field. Frozen in time, this population may bear information about the mechanism that brought it there.

We introduced the captured population into the Solar system and integrated it as test-particles together with the giant planets and the Galaxy's background potential over a timescale of 300 Myr[5]. The simulations are summarized in table 1. The resulting orbital parameters are presented in Fig. 6 as the brown dots. The thin black lines from each dot points to the orbital elements of that asteroid after 300 Myr.

During integration, the captured asteroids that were introduced in the conveyor belt-region have been driven by the giant planets into the Oort cloud region. The timescale on which they reach the Oort cloud depends on their relative inclination to the ecliptic, and on the pericenter distance. Highly inclined asteroids, for example, may have their closest approach to the Sun far from the perturbing influence of the giant planets. Asteroids orbiting in the ecliptic plane are more strongly affected by the giant planets, and are scattered into the conveyor belt on a shorter timescale.

3.3.4. When did the Sun escape the parent cluster?

We assumed that stars formed instantaneously with positions randomly from a point-symmetric Plummer (1911) potential in virial equilibrium. Planets also form instantaneously in almost circular orbits in a randomly oriented eclyptic plane.

These are strong (and honestly rather preposterous) assumptions, and some of our results for sure are affected by these choices. However, relaxing any of these assumptions will open-up parameter space and lead to a dramatic increase in the number of calculations required to acquire reliable uncertainties on the simulation results. One of these improvements would be to take the hydrodynamical collapse of the molecular cloud into account, including the processes of star formation, stellar feed-

[5] The time scale of 300 Myr was selected empirically. The migration time-scale for highly inclined asteroids turn out to be about 100 Myr (see Sect. 3.3.2), we therefore had to integrate for at least this time span. The calculations, however, are sufficiently expensive to not continue the them for too long.

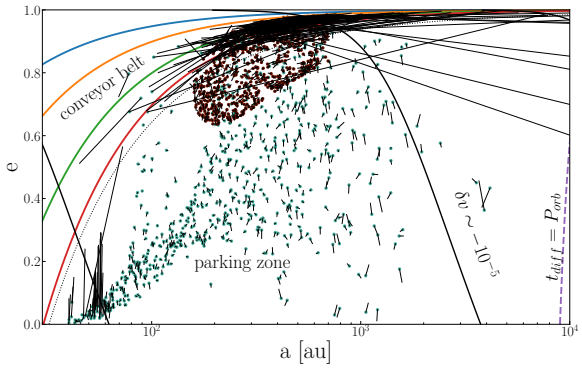

Fig. 6. Orbital distribution of the scattered (green dots) and captured (brown) asteroids. These conditions originate from the scatter and capture calculations, but form the initial conditions for subsequent calculations. The former are scattered from the circumstellar debris disk by a close encounter with another star in the parent cluster. The latter population is captured from another star with which the Sun interacted in its parent cluster. The simulations for both populations are described in Tab. 1. The small-thin black lines from each dot-point points in the direction to which the orbit migrates over 300 Myr (we adopted 300 Myr here for the presentation, although we realize that adopting 100 Myr would have been a more systematic choice). This data was acquired by integrating the Solar system in the tidal field of the Galaxy. The asteroids that orbit the outer and inner parking zones are hardly affected by the Galactic tidal field. Those near the conveyor belt are strongly affected by the giant planets and some eventually reach the Oort cloud. The thin black-dotted curve parallels the 2.5 Hill-radii to the right of Neptune's pericenter influence (solid red curve), and indicates the extent to which the planet still affects the asteroid's orbits. Simulation parameters are listed in table 1.

back, disk evolution and planet formation. These calculations, however, are somewhat elaborate (Calura et al. 2020; Fukushima & Yajima 2021).

Even though the processes discussed in this paper are fundamental, the timescales and efficiencies of the various processes are affected by the simulations' initial conditions (Adams et al. 2006). The time over which, and the order in which the giant planets form are important for the presented model and the efficiency at which asteroids are ejected in the Oort cloud. The conclusion on the early ejection of asteroids by the giant planets while the Sun was a cluster member remains largely unaffected. The Oort cloud will be prevented from forming so long as the Sun is a member of a star cluster (Higuchi & Kokubo 2015). Only after the Sun has left the birth cluster, it is possible to keep asteroids bound in orbits as wide as the current Oort cloud up to the Hill-radius in the Galactic potential.

It is not trivial to constrain the moment at which the Sun escaped its birth cluster. In the first $\lesssim 10$ Myr, the cluster is expected to have a relatively high density $\gtrsim 10^3\, M_\odot/\mathrm{pc}^{-3}$ (Lüghausen et al. 2012; Martínez-Barbosa et al. 2016; Pfalzner & Vincke 2020; Pfalzner et al. 2020). After that, the cluster expansion is driven by stellar winds, radiation feedback, and supernovae until it eventually dissolves in the Galaxy's tidal field. This latter phase in which the cluster dynamics is dominated by two-body relaxation and tidal stripping lasts for approximately 100 Myr (Adams et al. 2006; Stock et al. 2020). While the cluster expands with time, the local density gradually decreases, and the encounter rate drops (Baumgardt & Kroupa 2007; Cai et al. 2017). These time scales are all short compared to the formation timescale for Jupiter of $\lesssim 4$ Myr (Kruijer et al. 2017; Movshovitz et al. 2010; D'Angelo et al. 2021).

The Solar system may have survived this first dense phase rather unharmed to leave the cluster at a later stage, possibly around the cluster's half-life timescale. According to our calculations (but also see Kaib & Quinn 2008), it seems harder to grow a rich Oort cloud if the Sun stayed in the parent cluster for $\gtrsim 100$ Myr, because this corresponds to the time scale on which the ice-giant planets eject their local asteroids into the conveyor belt. We, therefore, argue that the Solar system might have been ejected from the parent cluster within ~ 20 or 50 Myr after birth.

The effect of a nearby encounter on the cold Kuiper belt may not have had a long-lasting impact, as this population might have regrown over time (Astakhov et al. 2005; Punzo et al. 2014; Moore et al. 2020). Other signatures of the difference between a few strong encounters and extended exposure to relatively weak perturbations are hard to quantify. We did not explore the long-term survival of the Solar system in its birth cluster and its possible consequences for the planetary disk's outer edge. It would be interesting to study this aspect, but these calculations are elaborate, and parameter space is extended.

3.4. Eccentricity damping of the asteroids in the Oort cloud

While the gas-giant and ice-giant planets launch asteroids further into the Oort cloud, the Galactic tidal field gradually becomes a stronger perturber. Eventually, when asteroids cross the purple-dashed curve in fig. 6 (far to the right, but better visible in figures 1 and 2) their orbits become strongly affected by the Galactic tidal field through von Zeipel-Lidov-Kozai resonance (von Zeipel 1910; Lidov 1962; Kozai 1962), (see Ito & Ohtsuka 2019, for a historical overview on the terminology)]. This leads to the damping of the eccentricity (as is also demonstrated in Vokrouhlický et al. 2019). In our simulations, this proceeds through a random walk in semi-major-axis and eccentricity but directed towards lower eccentricities. In figure 7 we illustrate this process with three asteroids from one of our simulations. These particles start in the narrow neck between 1000 au and 3000 au at an eccentricity $\gtrsim 0.998$ while they are kicked by one of the giant planets along the conveyor belt into the Oort cloud region. The tidal field of the Galaxy subsequently reduces the orbital eccentricity of these asteroids. This eccentricity-damping process proceeds as a random walk in eccentricity and orbital separation. The influence of the Galactic tidal field near the asteroid's apocenter may cause the orbital eccentricity to increase as well as decrease, whereas the semi-major axis is less strongly affected. The global trend is a reduction in eccentricity. Eventually, after a few 100 Myr, we find empirically that the cumulative probability density function for the eccentricity approaches $f(e) \propto (1-e^2)^{-2/9}$. In Fig. 8 we present the evolution in the Oort cloud's eccentricity distribution in the lower 4 curves. In table 3 we present the conditions for the simulations that support this section.

Asteroids in the disk start with almost circular orbits (uppermost blue curve in figure 8). In time, this distribution becomes more skewed to higher eccentricity, mainly due to the injection of objects into the conveyor belt (orange curve). The scattered and captured asteroid populations have, upon capture, a steeper eccentricity distribution (purple curve), which approaches the thermal distribution (dotted curve).

A fraction of the disk particles together with some of the scattered disk and captured asteroids migrate further along the

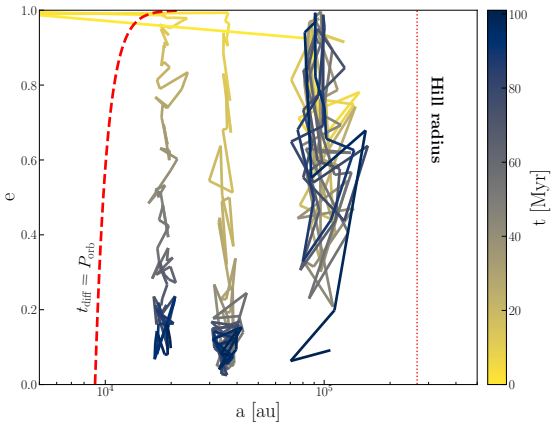

Fig. 7. Orbital evolution of three asteroids for 100 Myr in semi-major axis and eccentricity. Each started from the conveyor belt (to the top left) until they circularize. These asteroids are launched into the conveyor belt by a giant planet. This process is illustrated in fig 4. Once the Galactic tidal field starts to dominate the orbital evolution of the asteroids (to the right of the red-dashed curve), it detached them from the inner planets' influence. The Galactic tidal field subsequently drives the eccentricity evolution of the asteroid until it circularizes. The timescale of the circularization process is illustrated with the color bar. Asteroids further in the Oort cloud are more strongly affected by the Galactic tidal field, and therefore have a shorter circularization timescale. Not all asteroids circularize to the low eccentricities as the three examples presented here. The eventual eccentricity distribution of the Oort cloud objects is presented in figure 8. The vertical dotted curve to the right indicates the Hill radius of the Solar system in the Galactic potential.

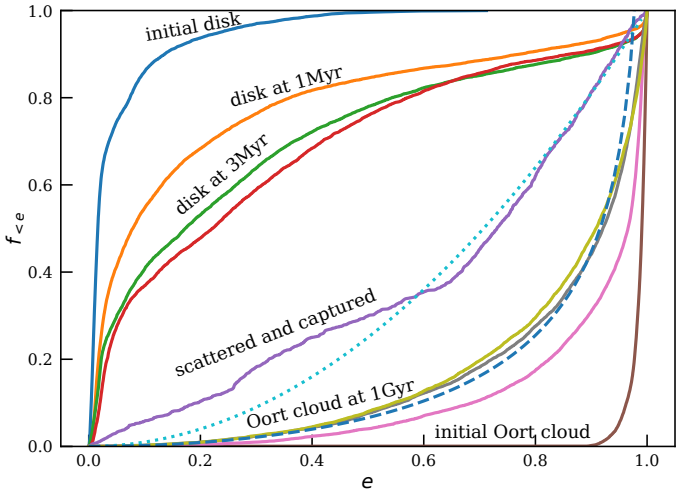

Fig. 8. Cumulative distribution of the eccentricity at various stages of the evolution of the eventual Oort-cloud population of asteroids. The dotted and dashed curves are presented to guide the eye. The dotted curve gives the probability density function for the thermal distribution in eccentricity ($f(e) \propto e^2$). The dashed curve gives an eccentricity probability density function $f(e) \propto (1-e^2)^{-2/9}$, which matches the eventual Oort cloud distribution at 1 Gyr. The top four curves give the eccentricity distribution of the initial disk around the Sun (see table 5), at the age of 1 Myr, 3 Myr and 10 Myr (red curve). The purple curve, through the middle of the figure, near the dotted curve, gives the distribution of the two populations of scattered disk objects and the captured asteroids (see also fig. 6 and table 1). Both the scattered and captured populations are comparable in number. The bottom four curves give the distribution of the Oort cloud asteroids, from bottom to top when the asteroids just enter the Oort cloud (indicated with "initial Oort cloud"), followed by the distribution at an age of 100 Myr, 500 Myr and 1 Gyr (as indicated, see also table 3). This figure contains data from simulations for which the parameters are listed in table 5 (top curves), 1 (middle purple curve), and 3 (bottom set of curves).

conveyor belt until their eccentricity distribution resembles the lowest (red) curve in figure 8. This latter distribution continues to evolve in time until it resembles the purple curve (indicated with the Oort cloud at 1 Gyr). Further evolution of the Oort cloud is slow, on a timescale of $\gtrsim 1$ Gyr, and dominated by evaporation. By counting the number of objects that re-enter the inner Solar system, we derive a rate of ~ 2–6×10^{-12} comets per asteroid in the Oort cloud per yr that find their way back into the inner Solar system within 10 au (see section 4.2.3). This leads to 1 or 2 comet arrivals in the inner Solar system per year, which is consistent with earlier estimates (Byl 1986; Heisler & Tremaine 1986; Gardner et al. 2011; Fouchard et al. 2020).

3.5. Summary of the chain of simulations

Now that we have briefly discussed each of the simulations, we can construct a more holistic view of the formation and early evolution of the Oort cloud. Here, we summarize this model and in the next section we discuss the consequences.

Asteroids in the conveyor belt cross the orbit of the giant planets. Each time this happens, they receive a small kick causing their orbits to drift with constant pericenter distance to higher eccentricity and larger semi-major axis (illustrated in figure 4, but see also Duncan et al. 1987). Jupiter ejects its nearby asteroids along this conveyor belt (indicated in Fig. 2) on a timescale of a few Myr.

Once the eccentricity of an asteroid $\gtrsim 0.998$ and its semi-major axis $\gtrsim 20\,000$ au the Galactic tidal field starts to dominate the asteroid's orbital evolution at apocenter (Higuchi et al. 2007, see fig 2). As soon as the pericenter distance exceeds the giant planet's semi-major axis, the eccentricity of the asteroids' orbit continues to be reduced. By this time, the orbital period is $\gtrsim 3$ Myr, and the Galaxy starts damping the asteroid's eccentricity and randomizing the inclination (Higuchi et al. 2007) on a timescale of ~ 100 Myr (Duncan et al. 1987; Di Sisto & Rossignoli 2020).

Eventually this process leads to the Oort cloud. The distance to which an asteroid penetrates the Oort cloud depends on the last interaction with the planets before its orbit detaches (see figure 7). Once near apocenter, the Galactic tidal field reduces the orbit's eccentricity, causing the pericenter distance to increase.

Our calculations did not last sufficiently long to circularize the entire population, but the reduction in eccentricity converged in ~ 1 Gyr to $f(e) \propto (1-e^2)^{-2/9}$. We, therefore, argue that the Oort cloud still hosts a considerable fraction of asteroids in relatively high-eccentricity orbits. This distribution in eccentricity is consistent with the one found in Higuchi & Kokubo (2015), at an age of 500 Gyr to 1 Gyr. They further argue that the eccentricity distribution in the Oort cloud thermalizes in ~ 5 Gyr. We do not observe such a thermalization of the eccentricity distritbuion. The structure of the Oort cloud can then also inform us about what happened in the early Solar system (see also Fouchard et al. 2018).

The orbital distribution of the giant planets is not very important in this evolutionary sequence, except that more massive planets, upon their last interaction, can inject asteroids in wider orbits with a higher eccentricity.

Jupiter's large mass and short orbital period clears the local asteroid field already in a few Myr (Duncan et al. 1987; Fouchard et al. 2014b). Hence, the Oort cloud cannot have formed from asteroids ejected by Jupiter and Saturn, because their ejection timescale is shorter ($\lesssim 10$ Myr) than the expected cluster lifetime of $\gtrsim 100$ Myr (Portegies Zwart et al. 2010). In Sect. 3.3.4 we concluded that the Sun escaped the parent cluster even before that time in 20 Myr to 50 Myr. In the first million years after their formation, the giant planets launch $\gtrsim 80.3\,\%$ of the asteroids between 3 and 15 au, onto the conveyor belt, and $57.0\,\%$ of these escape the Solar system within the next million years. Within ~ 10 Myr, all the asteroids born near Jupiter and Saturn are either deposited in resonances or escape the Solar system. Jupiter and Saturn therefore, cannot have contributed much to the formation of the Oort cloud (this was also concluded by Torres et al. 2020a,b). The details, however, depend on the relative timing of the various events and on the mass distribution within the disc. Constraining those more precisely would require more extended and sophisticated self-consistent simulations.

In our simulations, we ignore the star, planet, and asteroid-formation processes: all are born instantaneously. We have not explored parameter-space exhaustively, but argue that the details regarding the precise moment and the orbits in which the giant planets form are relevant only to second order because they affect the timescale for the formation of the Oort cloud but not the fundamental process.

There is sufficient slack in the various processes that the few Myr of planet-formation (Kruijer et al. 2017) does not pose a problem. So long as the Solar system is a member of a star cluster a sequence of distinct processes drive the formation of the Oort cloud.

4. Results and Discussion

4.1. The Solar system's birth environment

The birth environment of the Solar system plays a major role in the formation of the Oort cloud. It prevents the gas-giant planets from forming the Oort cloud, but at the same time stimulates its formation by scattering the outer regions of the circumstellar disk, and by introducing new asteroids by capturing them from other stars, or from the interstellar free-floating population (see also Zheng et al. 1990).

The Oort cloud has, according to this view, only a minor contribution from the scattered asteroids by the gas-giant planets, Jupiter and Saturn. Apart from those asteroids parked in resonant orbits, these planets cause asteroids to escape the Solar system. They become interstellar free-floating objects (see also Torres 2020; Torres et al. 2020a).

In contrast to Jupiter and Saturn, the ice giants, Uranus and Neptune, are more favorable in producing the Oort cloud (see also Leto et al. 2008; Paulech et al. 2010). They carry out the same process of ejecting asteroids, but do this, due to their lower mass and wider orbits, on a longer timescale and with smaller impulsive changes in eccentricity and semi-major axis of the asteroids (see also Duncan et al. 1987; Fernández et al. 2004; Correa-Otto & Calandra 2019).

The longer timescale on which the ice-giants planets eject asteroids is important for the formation of the Oort cloud because so long as the Solar system is a member of the parent cluster, asteroids in wide orbits are easily lost from the Solar system (Nordlander et al. 2017). This process of asteroid stripping due to encounters with nearby stars is particularly effective if the asteroid's orbit is wide and highly eccentric. After a few 10s of Myr to ~ 500 Myr, once the Solar system escaped the parent cluster, such asteroids can remain bound.

The wide and highly eccentric orbits of new arrivals in the Oort cloud can subsequently be perturbed at apocenter by the Galactic tidal field, leading to a reduction in their eccentricity through von Zeipel-Lidov-Kozai resonance. As a consequence, the pericenter distance of these asteroids increases, which brings them outside the influence of the planets and detaches them from the conveyor belt. While the orbital eccentricity of the asteroids continues to decay due to the Galactic tidal field, they slowly, over a timescale of ~ 100 Myr, form a distribution of very wide but relatively low-eccentricity orbits The distribution has to shape of the tidal lobe of the Solar system in the Galactic potential. The size of the Oort cloud is confined on the inner side to the distance where the Galaxy starts to influence the orbits (at a relative velocity change of $\delta v \gtrsim 10^{-3}$ of the asteroids and on the Hill's surface far side from the Sun in the Galactic potential (illustrated in figure 1 and figure 5).

According to Leto et al. (2008) the number density in the Oort cloud is proportional to $n \propto r^{-3.53}$, whereas we find a considerably more complex structure. In the Hills cloud and Oort cloud we find $n \propto r^{-2.25}$, with an overall flatter slope of -2.57 for the entire range from 100 au to the Hills radius (see figure 9). The slope of the density profile of ~ -2.25 between 2×10^4 au and 10^5 au is somewhat shallower than the slope of but steeper than the slope of ~ -4.0 by Higuchi & Kokubo (2015), ~ -3.35 found by Vokrouhlický et al. (2019) or ~ -3.0 by Leto et al. (2008). Higuchi & Kokubo (2015) argue that this slope is independent of the mechanism that brings asteroids to the Oort cloud, but that does not explain the differences in the density profile between these different studies. Part of this structure may be the result of orbital evolution of the Solar system and its possible migration in the Galaxy (Rickman et al. 2008; Kaib et al. 2011a,b), but another part may be the result of planetary migration (Fouchard et al. 2018).

4.2. Results

4.2.1. The Sun in the Galaxy

A small fraction ($\sim 0.59 \pm 0.1$ percent of the Oort cloud population) on the far side of the Hill sphere remains bound to the Sun (see figure 9). At an age of 1 Gyr in our simulations, this population has an eccentricity of $\langle e \rangle = 0.80 \pm 0.23$ with an inclination of $\langle i \rangle = 96^\circ \pm 42$. These orbital parameters are rather similar to those of the Oort cloud asteroids within the Sun's Hill surface, and they are consistent with the population presented in figure 7 of Vokrouhlický et al. (2019). They tend to be physically at the far side of the Hill sphere (beyond ~ 200000 au), but not expected to stay there long as they are ionized from the Solar system by close stellar passages in the Galactic field (Correa-Otto & Calandra 2019).

Asteroids ejected from the Solar system become free-floating interstellar objects. This latter population forms a trail of asteroidal objects in the Galaxy along the parent star's orbit (Correa-Otto & Calandra 2019; Torres et al. 2020a; Portegies Zwart 2021). Since the asteroids have a low velocity relative to the Solar system's orbital speed, they continue to follow the same orbit as the Sun (see fig. 3). Long after they have become unbound, these asteroids still orbit in a cloud around the Solar system distributed along extended trailing and leading arms. Eventually, these trails may be perturbed and scattered by passing molecular clouds or other stars, scattering their orbits and widening

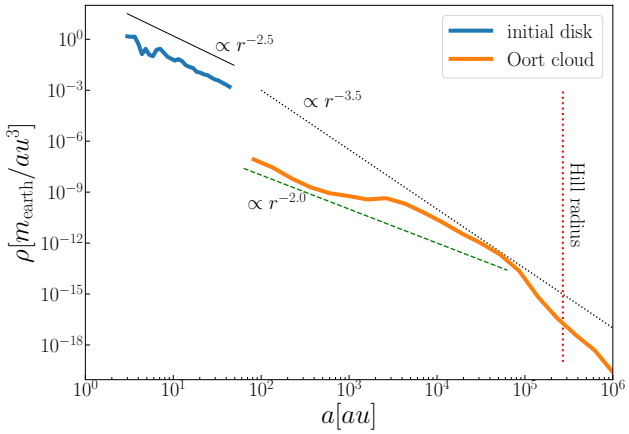

Fig. 9. Density profile of the initial circumstellar debris disk (blue, to the top left) and the eventual Oort cloud, ~ 1 Gyr after the Solar system left the parent cluster (orange). The red dotted line to the right indicates the formal Hill radius of the Sun in its orbit around the Galactic center. The thin-solid black-dotted curve shows the initial density profile of the circumstellar disk of $\propto r^{-2.5}$ (from simulations of Tab. 3). The thin dotted curve shows the density profile $\propto r^{-3.5}$ which, according to Leto et al. (2008), resembles is the slope of the density profile of the Oort cloud. In our calculations, the distribution is somewhat shallower, but not as shallow as found in Higuchi & Kokubo (2015) who argue in favor of $\propto r^{-2.0}$, which is presented in the figure with the green dashes. The small tail of asteroids beyond the Solar system's Hill radius in the Galactic tidal field has contributions of a minority of asteroids that remain bound to the Sun, and those that slowly move away.

their phase-space distribution (see Martínez-Barbosa et al. 2016; Pfalzner et al. 2020; Torres et al. 2020a).

4.2.2. Consequences of planets in resonant orbits

We perform several additional simulations to study the consequences of planet migration in the early Solar system. In tables 5, and 6 we present an overview of these calculations. Apart from the currently observed distribution of orbits for the giant planets, we also simulate more compact and a resonant configuration. The main problem in exploring these initial conditions hides in the enormity of the initial parameter space to cover; Our parameter-space coverage is far from complete. We therefore selected a few cases which have been of some interest in the past (see e.g. Wyatt 2003; Gomes et al. 2005; Malhotra 1998; Crida et al. 2007; Brunini 2019).

In one of these cases, we initiate a Nice-like planetary orbital distribution and a disk between 3 au and 50 au. In that configuration, Jupiter was placed on a circular orbit at 5 au in the ecliptic plane, and the subsequent planets in 2:1 mean-motion resonances with the one closer to the star. We also tried other configurations (see Tab. 3). The main conclusions, that the gas-giant planets (Jupiter and Saturn) eject asteroids on a timescale shorter ($\lesssim 10$ Myr) than the expected survival timescale in the parent cluster ($\gtrsim 100$ Myr), holds also for these initial conditions.

Changes in the orbital distribution of the giant planets affect the location and efficiency of the conveyor belt, and the timescale on which asteroids migrate along the conveyor belt. In our initial resonant configuration, the entire disk, up to the orbit of the outermost planet, at around 15 au, is cleared within 1 Myr. The area slightly outside the outermost planet, up to a distance of 20 au from the star, is cleared within a few million years. By the time the Solar system leaves the parent cluster, there are too few asteroids left for populating the Oort cloud.

Pirani et al. (2019) also simulated the early Solar system including the migration of the giant planets. Although they focused on the inner Solar system and the populations of resonant and Trojan orbits, their conclusions are consistent with the results of the calculations presented here. Planets in an initial resonant configuration are excluded based on the consequence that the majority of asteroids would be lost well before the Sun escapes the parent cluster. This also accounts for Uranus and Neptune; if they are born in (near) resonance, the chaotic reorganization of the Solar system would eject most of the asteroids in the disk on a timescale shorter than the expected lifetime of the Sun in the parent star cluster. Asteroids outside the outer most planet will be affected by resonant reorganization of the planetary orbits, but these asteroids are not likely to migrate into the conveyor belt, and therefore are not expected to arrive in the Oort cloud. Fully resonant initial conditions can then be omitted based on the existence of the Oort cloud, except for the part of the Oort cloud material was accreted from other stars or from free-floating debris.

Even if a resonant configuration in the ice-giant planets would lead to a dramatic change in the distribution of orbital parameters after ~ 100 Myr, as is advertised in the original Nice model (Gomes et al. 2005; Morbidelli et al. 2005; Tsiganis et al. 2005), the amount of asteroids has already reduced below the number needed to explain the Oort cloud. We, therefore, argue that a system in which the planets are born close to resonance, or in which planets migrate in the first few Myr since formation (such as advertised in the grand-tack model Walsh et al. 2011), is unlikely to lead to the formation of an Oort cloud. Planetary migration after the Oort cloud formed has no further consequence for the Oort cloud, and we cannot exclude such evolution (Valtonen & Innanen 1982). But again, resonant initial conditions for the planets can not be excluded if the majority of Oort-cloud material was accreted.

4.2.3. Retrograde and re-entry orbits

We measure the fraction of asteroids in retrograde orbits. At the age of 300 Myr well after the Sun escaped the cluster, $8.1 \pm 0.3\%$ of the scattered asteroids ($a \gtrsim 100$ au) have retrograde orbits, and for the compact resonant initial conditions this fraction is $7.1 \pm 0.5\%$. In comparison to $71.9 \pm 0.3\%$ of the captured asteroids ($a \gtrsim 100$ au) have retrograde orbits. The latter fraction, however, sensitively depends on the encounter parameters and the number may vary considerably for other simulations. Once well along the conveyor belt (at $a(1-e) \gtrsim 50$ au and eccentricity $\gtrsim 0.998$), about 57 ± 1 % of the asteroids have retrograde orbits. This large fraction of retrograde orbits in the conveyor belt indicates the moment that the Oort cloud becomes spherical and isotropic. By this time, the orbits have also reached their terminal distribution in eccentricity (which is not thermal, see fig 8).

Due to interaction with the tidal field, a small fraction of asteroids return to the inner Solar system after having spent some time in the Oort cloud. We find $0.6 \pm 0.1\%$ of the asteroids that were launched from the conveyor belt into the Oort cloud return into the inner 10 au of the solar system on a timescale of 1 Gyr. This results in a re-entry rate of 2 to 6×10^{-12} yr^{-1}. The re-entry rate for approaching the Sun to within 1 au is an order of magnitude smaller. The observed rate of observable comets in the Solar system, measured between 110 BC and 1970, was remarkably constant at a rate of 0.86 ± 0.067 per year (Licht 1999). A larger rate of 6.4×10^{-12} per year was derived by Dones

Planets born in orbital resonance (see sect. 4.2.2)	
Designation	Simulation D.
Simulations	1 simulation with planets (in various configurations), asteroids and Galactic tidal field.
Star	Single 1 $M_\odot$ with 4 giant planets, 10000 asteroids in the smooth potential of the Milky Way Galaxy.
Planets	The 4 planets have almost circular orbits ($e < 0.006$) in the plane ($i < 0.1°$) with Jupiter, Saturn, Neptune and Uranus in orbits with semi-major axis of 5.1, 9.5, 19.2, 30.1 au. The ecliptic was inclined with $60°$ to the Galactic plane. We performed two more simulations with initial semi-major axis 3.75, 5.953, 9, 449, 15.0 au, and with semi-major axis of 5.5, 8.1, 11.5, 14.2 au for the four giant planets.
Asteroids	10000 asteroids in circular orbits between 3 au and 50 au in a thick disk (Toomre-Q parameter of 25 Toomre 1964) in the plane of the planets.
Numerics	`Huayno` (Pelupessy et al. 2012) coupled to the Galactic model see table 4 via bridge (Portegies Zwart et al. 2020) in AMUSE (Portegies Zwart & McMillan 2018).
Computer	run on LGM-II with GPU
Duration	simulation performed for a duration of 1 Gyr.

Table 5. Simulations of a hypothetical young Solar system with planets in various orbital configurations.

Planets born in orbit around an isolated star (see sects. 3.2 and 4.2.2)	
Designation	Simulations E.
Simulations	12 simulation to study the internal planetary dynamics and their response to the local asteroids.
Star	Single 1 $M_\odot$ with 4 planets, 2000 asteroids.
Planets	4 planets in almost circular orbits ($e < 0.006$) in the plane ($i < 0.1°$) with Jupiter, Saturn, Neptune and Uranus in orbits with semi-major axis of orbits with semi-major axis of 5.1, 9.5, 19.2, 30.1 au. We performed two more simulations with initial semi-major axis 3.75, 5.953, 9, 449, 15.0 au.
Asteroids	2000 asteroids in circular orbits in a thick $Q = 25$ disk in the ecliptic plane of the planets between 3 au and 50 au.
Numerics	`Huayno` (Pelupessy et al. 2012)
Computer	run on a 192 core Intel-Xeon workstation.
Duration	simulation performed for a duration of 50 Myr.

Table 6. Simulations of the young Solar system.

et al. (2004a), but they accounted for perturbations in the Oort cloud due to passing stars, which we neglected in our calculations. With our derived re-entry rate of comets within an astronomical unit of the Sun of $\sim 6 \times 10^{-13}$ yr^{-1}, and a total number of $\sim 10^{12}$ cometary bodies in the Oort cloud, we derive a rate of about two new comets every 3 years. Even when taking the tidal field and passing stars into account, our derived rate is somewhat on the low side compared to the observations. The presence of a planet in the Oort cloud would pose an interesting possibility in increasing the cometary influx rate (Fouchard et al. 2014a; Ito & Higuchi 2020; Batygin & Brown 2021).

4.3. Interstellar comets

According to the simulations presented here, the Solar system is a copious polluter of interstellar space (Torres et al. 2019; Pfalzner et al. 2021); interstellar comets produced in this way could have characteristics similar to 'Oumuamua or Borisov (Higuchi & Kokubo 2020). This pollution predominantly happens in four rather distinct phases in the evolution of the Solar system:

A while being a cluster member, when encounters between stars cause debris from the crircustellar disk to escape,
B while the giant planets (Jupiter and Saturn) eject most the of the asteroids in their gravitational influence,
C After the Sun ascaped the cluster, and the ice giant planets (Uranus and Neptune) start kicking out asteroids,
D and eventually due to the Sun's copious mass loss while ascending the asymptotic giant branch and evolving into a white dwarf, causing asteroids to become unbound (Veras et al. 2011; Veras & Tout 2012; Veras et al. 2014, 2020).

According to Cai et al. (2019) 20–80% (with an average of 50 %) of the circum-stellar material survives the first 100 Myr of its evolution in the parent cluster. The majority of this mass is lost through encounters with other stars. The amount of material lost from the solar system in the simulation presented here falls in this rage, meaning that the circumstellar disk has lost about half it's mass due to interactions with other stars in the parent cluster, or about 100 $M_\oplus$ to 3000 $M_\oplus$. Each of the other processes results in a mass loss of roughly 20%. A small fraction of the ejected asteroids acquire a bound orbits in the Oort cloud.

With an estimated mass of the Oort cloud of $\sim 10^{13}$ kg/comet, and a Hill radius of ~ 0.65 pc, we arrive at a density of $\sim 10^{14}$ kg/pc^3. If the Solar system has ejected ~ 90 % of its asteroids into interstellar space, rather than forming an Oort cloud, interstellar space would have an average density of a few times $\sim 10^{14}$ kg/pc^3. This estimate is consistent with earlier estimates for the interstellar density of interstellar objects (Portegies Zwart et al. 2018; Do et al. 2018; 'Oumuamua ISSI Team et al. 2019)

Regretfully, backtracking a single interstellar interloper to its origin is hindered by the uncertainties in the orbital parameters and the positions of stars in the past. Such backtracking is limited to at most a few tens of millions of years Zhang (2018).

However, if multiple objects were found to have the same origin, backtracking the orbit could lead to a more precise determination of the original launching point (Portegies Zwart 2021). According to our calculations, however, most objects will have been ejected at an early stage while planets are still forming

and migrating (see also Pirani et al. 2019). Possibly the star is even still a cluster member, in which case internal scattering with other stars will make it hard to trace back the interstellar object to a single star.

4.4. Discussion

4.4.1. Interpretations and caveats in the numerical approach

Numerical simulations are always affected by choice of initial conditions, and by numerical errors; either from the discretization of the underlying differential equations or by the exponential growth of round-off in the least significant digit. And then, we did not even mention the possibility of bugs.

These uncertainties and errors become a particular potential cause of concern in chaotic systems. The outer parts of the Solar system, for example, has an estimated Lyapunov timescale ranging from $\lesssim 20$ Myr (Applegate et al. 1986; Sussman & Wisdom 1988; Laskar 1990; Sussman & Wisdom 1992; Murray & Holman 1999; Farrés et al. 2013), to as much as 50 Myr (Laskar et al. 2011) or even exceeding the age of the Solar system (Grazier et al. 1999; Varadi et al. 2003).

Choices made in the initial conditions have considerable consequences for the numerical results and their interpretation. At the same time, numerical errors also will have their repercussions on the conclusions in section 5. Similar caveats in numerical work ware already acknowledged by Charles Babbage (1791-1871), inventor of the difference and the analytical engines, who remarked:

> On two occasions I have been asked, — "Pray, Mr. Babbage, if you put into the machine wrong figures, will the right answers come out?" ... I am not able rightly to apprehend the kind of confusion of ideas that could provoke such a question.

Aware of these and other limitations, we describe the caveats in our approach in this section and discuss how to mitigate them.

4.4.2. Integration, symplecticity and numerical errors

Newton's equations of motion are intrinsically chaotic. Planetary systems are therefore also chaotic, just like the Solar system (Lecar et al. 2001; Valtonen et al. 2004). Chaos in the outer parts of the Solar system manifests itself as phase-bound or stable chaos (Milani & Nobili 1992; Saillenfest et al. 2019) and, although it affects the stability of the Solar system (Todorović et al. 2020), it will not lead to a global unstable configuration (Tanikawa & Ito 2007). Chaos in the solar system is driven by resonance overlap (Murray & Holman 1999, 2001). Even the Oort cloud is chaotic (Saillenfest et al. 2019).

Such chaos hinders the integration of the equations of motion for the Solar system. It renders these simulations notoriously unreliable for individual orbits. Possibly statistically they are trustworthy, meaning that the integrated bodies preserve the same phase space, but this has never been tested (for a discussion see Portegies Zwart & Boekholt 2018).

In this paper and many others, we rely on the statistical ensemble averaging by numerical integration. The folklore in these simulations is that the conservation of energy is sufficient to preserve the final orbital parameter space. Symplectic integration methods are developed with precisely this objective, to preserve energy over secular time scales. Therefore, these methods are popular for integrating planetary systems (Ito & Tanikawa 2002), but not so much for integrating star clusters or galaxies.

Although details in our calculations will depend on precise initial realization of the giant planets, the general results remain unaffected. We tested the effect of rather drastic variations on the initial conditions, and the effect of subtle changes (like the Solar system's Epoch), but we did not explore these systematically. The various simulation codes to perform this study are public via the AMUSE framework, and we encourage others to continue exploring parameter space.

5. Summary and conclusions

Shortly after their birth, Jupiter and Saturn start to eject local asteroids from the circumstellar disk along the 'conveyor belt'. Asteroids in the conveyor belt cross the orbit of the giant planets near their pericenter. Each time this happens, they receive a small kick causing their orbits to drift to higher eccentricity and larger semi-major axis while preserving pericenter distance. This process has been studied for asteroids with their pericenter near Jupiter (Duncan et al. 1987; Fernández 1997). We confirm that Jupiter, with its relatively high mass and short orbital period, clears the local asteroid field in a few Myr (Fernández 1997; Pirani et al. 2019). In figure 4, we illustrate the process by presenting one calculation where a single asteroid is ejected along the conveyor belt to reach the Oort-cloud region in a few Myr. For the ice giants, however, with their smaller mass and wider orbits, the process takes up to ~ 100 Myr (Fernandez 1981; Fouchard et al. 2013; Di Sisto & Rossignoli 2020), and if the asteroid has an inclined orbit, the process may last a Gyr.

While a member of a star cluster, an asteroid in a wide $\gtrsim 10^3$ au orbit is easily lost from the Solar system. A small perturbation in relative velocity of $\delta v \equiv dv/v \geq \mathcal{O}(10^{-4})$, is sufficient to unbind an asteroid. It turns out that asteroids on an eccentric orbit ≥ 0.98 and with semi-major axis $\gtrsim 2400$ au are vulnerable to being stripped from the Solar system. The period of such a wide orbit ($\gtrsim 0.1$ Myr) is comparable to the mean encounter-time between the Sun and another star in the parent cluster (assuming that the encountering star induces a similar perturbation in relative velocity). In the first million years since their formation, the giant planets launch ~ 80 % of the asteroids between 3 and 15 au onto the conveyor belt (see section 3.5). Once there, the eccentricity and orbital separation of the asteroids rapidly increases.

The majority of the asteroids are moving along trajectories that become so wide that they are stripped within a few orbits (~ 57 %), within a few orbits, and within ~ 10 Myr most of the asteroids born near Jupiter and Saturn are either parked in resonant orbits (such as the Hilda family of asteroids) or their orbits have become so wide that they are easily stripped by passing stars in the parent cluster, and escape in about 20 to 50 Myr.

The Oort cloud therefore cannot have formed in the first 10 Myr by Jupiter and Saturn ejecting asteroids because their ejection timescale is smaller than the timescale on which the Solar system is expected to be ejected from the parent cluster ($\lesssim 100$ Myr). This statement is unaffected by the few-Myr formation timescale for the giant planets.

Before escaping the cluster, stars in our simulations experience multiple encounters. The dynamic signature of multiple encounters on the outer regions of a planetary system is distinctly different from that of a single strong encounter (Hands et al. 2019). The outer parts of the solar system has signatures of both: A single strong encounter with another star can explain the Kuiper-cliff (Punzo et al. 2014) and the orbit of Sedna

(Shankman et al. 2011; Jílková et al. 2015), but the complex distribution of orbital parameters in the scattered Kuiper-belt beyond ~ 45 au (Kobayashi et al. 2005) seems best explained with a series of relatively weak encounters (see Brasser et al. 2012; Breslau et al. 2017; Hands et al. 2019; Moore et al. 2020, and section 3.3.2). We therefore argue that the Solar system was affected by multiple encounters in its parent cluster, until a strong encounter caused it to escape.

In our simulations, multiple interactions lead to $\sim 5\,\%$ of the asteroids in the outer disk, beyond 45 au, to be scattered into the conveyor belt region (see section 3.3.2). But the Sun also captures material from the disks of the stars it encounters. The efficiencies at which material is transported from one star to another is rather symmetric (Bhandare et al. 2016). The scattered and captured populations are comparable in number, but populate different regions in orbital parameter-space around the Sun.

In a reconstruction of the encounter that brought Sedna into the Solar system as a captured asteroid from the disk of another star, $\sim 28\%$ of the captured asteroids are injected directly into the conveyor belt region (see figure 1, of Jílková et al. 2015, and section 3.5). The high inclination of the scattered and captured populations, compared to the native disk, causes them to interact less efficiently with the giant planets. These asteroids reach the Oort cloud on a timescale of ~ 1 Gyr. Due to this long timescale, they lurk around in the parking zone of the Solar system where they are protected against being ejected by passing stars. Once the Sun is isolated, asteroids in the conveyor belt escape the Solar system only if their apo-center distance exceeds the Hill-radius of the Solar system in the Galactic potential, at ~ 0.65 pc, or $\delta v \gtrsim 0.1$.

Before an asteroid reaches such a wide orbit, it is subject to eccentricity-damping by the Galactic tidal field via von Zeipel-Lidov-Kozai oscillations (von Zeipel 1910; Lidov 1962; Kozai 1962). The relatively high inclination of the ecliptic to the Galactic plane (of $\sim 60^\circ$) helps to circularize their orbits and randomize their inclinations (Higuchi et al. 2007). The von Zeipel-Lidov-Kozai process causes the pericenter of the asteroid's orbit to detach from the planetary region (Higuchi et al. 2007), preventing it from being kicked out by a planet. Both processes, the ejection by the giant planets as well as the eccentricity-damping by the tidal field are essential ingredients that operate on comparable timescales. Once the Galactic tidal field reduces the eccentricity below 0.998 and the semi-major axis $\gtrsim 20\,000$ au ($a(1-e) \gtrsim 50$ au, to the right of the dashed curve in figure 2), the driving force that pumps the asteroid's orbit further into the conveyor belt switches off. By this time, the asteroid is detached from the inner Solar system.

The ejection of the native, scattered and captured asteroids along the conveyor belt, and their subsequent eccentricity-damping by the Galactic tidal field leads to the formation of the Oort cloud some 100 Myr after the Sun escaped the parent cluster (Kaib & Quinn 2008). The effect of passing stars in the parent cluster, and planet-asteroid interaction together with the Galactic tidal field are essential ingredients that contribute to define the orbital structure of the outer Kuiper belt, the Hills sphere and the Oort cloud. In figure 2, we illustrate the orbital parameter-space at this instance (see also section 3.5).

The conveyor belt beyond the ice-giant planets is further depleted in the next few 100 Myr, resulting in the clearing of the asteroids beyond Saturn's orbit and providing material for the Oort cloud. This could explain for the dearth of Centaurs in the Solar system without requiring a chaotic reorganization of the ice-giant planets (Fouchard et al. 2014b).

Based on our calculations, $\sim 5\,\%$ of the asteroids in the Oort cloud originate from the outer disk, beyond ~ 45 au. About one third ($\sim 30\%$) is captured from another star, and the rest originates from the circumstellar disk between ~ 15 au and 45 au. The majority of scattered and captured asteroids never make it to the Oort cloud, but linger around in the parking zone, between the two solid curves indicated with $\delta v \sim 10^{-8}$ and $\delta v \sim 10^{-5}$ in fig. 2 and fig. 6, or scape the Solar system. These captured objects should still be there and can be identified based on their unorthodox orbits and composition. The difference in the color of Kuiper belt and Oort-cloud objects indicate that are not related (Jewitt 2002). Once in the Oort cloud, the origin of an asteroid can be established on its kinematics, because of the phase-mixing driven by the chaotic process that injected them into the Oort cloud menifests itselfs on a time-scale longer than the Solar system's lifetime. The outer Solar-system origin of these asteroids can possibly be established by spectral analysis, much in the same way as C/2019 Q4 (Borisov) was analyzed using the OSIRIS (de León et al. 2019) and MUSE (Bannister et al. 2020) instruments. One of the remarkable findings is the depletion of C_2 (Opitom et al. 2019) and NH_2 (Bannister et al. 2020).

The presented scenario for the formation of the Oort cloud is rather insensitive to the details of the orbits of the outer planets. Asteroids can be launched into the conveyor belt to reach the Oort cloud from the current orbital distribution of the giant planets, or from a chaotic migration of the ice-giant planets. If, however, any chaotic reorganization or migration of the giant planets would happen before the Sun escaped the parent cluster, the Oort cloud would contain considerably fewer objects because most asteroids would escape. In addition, the orbital distribution of objects in the Oort cloud would be different (Shannon et al. 2019).

We continued our calculations for 1 Gyr, but already after a few 100 Myr the Oort cloud is fully formed, and the eccentricity distribution approaches a probability distribution $f(e) \propto (1-e^2)^{-2/9}$ (see sect. 3.3.3) with a density distribution $\propto r^{-3}$ (see sect. 4.1).

By this time, the Solar system is surrounded by a cloud of unbound asteroids which co-move along the Sun's orbit in the Galaxy. This co-moving group contains $\gtrsim 10^{11}$ comet-mass asteroids, most of which originated from the inner Solar-system. This unbound population is illustrated in figure 3. If other stars have Oort clouds of their own, the Solar system moves through a sea of Oort-cloud objects that originally belonged to other stars (see also Torres et al. 2020a; Portegies Zwart 2021).

The Oort cloud gradually evaporates with a half-life of about 1 Gyr due to the tidal field's kinematic heating and passing stars. Lost objects become free-floating asteroids in interstellar space (Torres et al. 2019), much like 'Oumuamua and Borisov.

Interaction with the Galactic tides also causes asteroids to be launched into the inner Solar system, where they can be observed as comets. In our simulations, the rate at which Oort cloud objects re-enter the inner Solar system (to within 1 au) is 0.2—0.6 per year (see section 4.2.3), which is somewhat lower than the empirical estimate of 0.86 ± 0.07 per year (Licht 1999). But here we ingnored the possible ionizing effect of passing stars in the Galactic potential.

Energy consumption of this calculation

Being concerned about the polluting influence of our science (Burtscher et al. 2020; Portegies Zwart 2020) we would like to raise awareness of the environmental impact of our calculations. We run AMUSE for about 40000 single-core CPU

hours. This results in about 2MWh of electricity http://green-algorithms.org/), consumed by the Dutch National supercomputer. With our estimate on the proportion of green electricity used, produced $\sim$ 530 kg CO2, which is comparable to driving a car from Leiden to Kars. The same data, however, was also used to perform other research, and we argue that less than half the CO2 produced in these calculations should be attributed to this paper.

Public data

The source code, input files and simulation data for this manuscript are available at 10.6084/m9.figshare.13214471. A tutorial on how to run the various codes in AMUSE is available at https://github.com/spzwart/AMUSE-Tutorial.

Software used for this study

This work would have been impossible without the following public open source packages and libraries: Python (van Rossum 1995), matplotlib (Hunter 2007), numpy (Oliphant 2006), MPI (Gropp et al. 1996; Gropp 2002), ABIE (Cai 2018, see https://github.com/MovingPlanetsAround/ABIE), NBODY6++GPU (Wang et al. 2015) and REBOUND (Rein & Liu 2012), SeBa (Portegies Zwart & Verbunt 1996; Toonen et al. 2016), and AMUSE (Portegies Zwart et al. 2018, available for download at https://amusecode.org).

Acknowledgments

It is a pleasure to thank Diptajyoti Mukherjee, Fransisca Concha-Ramírez, $\ln(a)$ Sellentin, Julia Wasala, Eiichiro Kokubo, Ramon Brasser and Tim de Zeeuw for discussions. We also thank the anonymous referee(s) for valuable comments on on the manuscript. We are grateful for the support of the Mexican National Council for Science and Technology (CONACYT) grant #291004-410780. This work was performed using resources provided by the Academic Leiden Interdisciplinary Cluster Environment (ALICE), LGM-II (NWO grant # 621.016.701) and the Dutch national e-infrastructure with the use of the Dutch national supercomputer Cartesius, and the support of SURF Cooperative.

References

Adams, F. C. 2010, ARA&A , 48, 47
Adams, F. C., Hollenbach, D., Laughlin, G., & Gorti, U. 2004, ApJ , 611, 360
Adams, F. C., Proszkow, E. M., Fatuzzo, M., & Myers, P. C. 2006, ApJ , 641, 504
Alexandersen, M., Benecchi, S. D., Chen, Y.-T., et al. 2019, ApJS , 244, 19
Allen, C. W. 1973, Astrophysical quantities
Alvarez, W. & Muller, R. A. 1984, Nat , 308, 718
Applegate, J. H., Douglas, M. R., Gursel, Y., Sussman, G. J., & Wisdom, J. 1986, AJ , 92, 176
Astakhov, S. A., Lee, E. A., & Farrelly, D. 2005, MNRAS , 360, 401
Bailer-Jones, C. A. L. 2009, International Journal of Astrobiology, 8, 213
Bannister, M. T., Opitom, C., Fitzsimmons, A., et al. 2020, arXiv e-prints, arXiv:2001.11605
Batygin, K., Adams, F. C., Brown, M. E., & Becker, J. C. 2019, PhysRep , 805, 1
Batygin, K. & Brown, M. E. 2016, AJ , 151, 22
Batygin, K. & Brown, M. E. 2021, ApJL , 910, L20
Baumgardt, H. & Kroupa, P. 2007, MNRAS , 380, 1589
Beckwith, S. V. W., Sargent, A. I., Chini, R. S., & Guesten, R. 1990, AJ , 99, 924
Bernardinelli, P. H., Bernstein, G. M., Sako, M., et al. 2020, The Planetary Science Journal, 1, 28
Bhandare, A., Breslau, A., & Pfalzner, S. 2016, A&A , 594, A53
Boehnke, P. & Harrison, T. M. 2016, Proceedings of the National Academy of Sciences, 113, 10802
Boehnke, P. & Harrison, T. M. 2018, LPI Contributions, 2107, 2033
Bottke, W. F., Nesvorný, D., Vokrouhlický, D., & Morbidelli, A. 2010, AJ , 139, 994
Bottke, W. F. & Norman, M. D. 2017, Annual Review of Earth and Planetary Sciences, 45, 619
Brasser, R. 2008, A&A , 492, 251
Brasser, R., Duncan, M., & Levison, H. 2007, Icarus, 191, 413
Brasser, R., Duncan, M. J., & Levison, H. F. 2006, Icarus , 184, 59
Brasser, R., Duncan, M. J., Levison, H. F., Schwamb, M. E., & Brown, M. E. 2012, Icarus , 217, 1
Brasser, R., Higuchi, A., & Kaib, N. 2010, A&A , 516, A72
Brasser, R. & Schwamb, M. E. 2015, MNRAS , 446, 3788
Breslau, A., Steinhausen, M., Vincke, K., & Pfalzner, S. 2014, A&A , 565, A130
Breslau, A., Vincke, K., & Pfalzner, S. 2017, A&A , 599, A91
Brown, M. E. 2001, AJ , 121, 2804
Brown, M. E., Trujillo, C., & Rabinowitz, D. 2004, ApJ , 617, 645
Brucker, M. J., Grundy, W. M., Stansberry, J. A., et al. 2009, Icarus , 201, 284
Brunini, A. 2019, MNRAS , 483, 5042
Burtscher, L., Barret, D., Borkar, A. P., et al. 2020, Nature Astronomy, 4, 823
Byl, J. 1986, Earth Moon and Planets, 36, 263
Cai, M. 2018, Moving Planets Around (MPA) Project
Cai, M. X., Kouwenhoven, M. B. N., Portegies Zwart, S. F., & Spurzem, R. 2017, MNRAS , 470, 4337
Cai, M. X., Portegies Zwart, S., Kouwenhoven, M. B. N., & Spurzem, R. 2019, MNRAS , 489, 4311
Cai, M. X., Portegies Zwart, S., & van Elteren, A. 2018, MNRAS , 474, 5114
Calura, F., Bellazzini, M., & D'Ercole, A. 2020, MNRAS , 499, 5873
Chebotarev, G. A. 1965, SvA , 8, 787
Chiang, E. I., Jordan, A. B., Millis, R. L., et al. 2003, AJ , 126, 430
Clarke, C. J. 2007, MNRAS , 376, 1350
Clarke, C. J. & Pringle, J. E. 1993, MNRAS , 261, 190
Concha-Ramírez, F., Wilhelm, M. J. C., Portegies Zwart, S., van Terwisga, S. E., & Hacar, A. 2021, MNRAS , 501, 1782
Correa-Otto, J. A. & Calandra, M. F. 2019, MNRAS , 490, 2495
Crida, A. 2009, ApJ , 698, 606
Crida, A., Morbidelli, A., & Tsiganis, K. 2007, in European Planetary Science Congress 2007, 866
Cuello, N., Dipierro, G., Mentiplay, D., et al. 2019, MNRAS , 483, 4114
D'Angelo, G., Weidenschilling, S. J., Lissauer, J. J., & Bodenheimer, P. 2021, Icarus , 355, 114087
Davis, M., Hut, P., & Muller, R. A. 1984, Nat , 308, 715
de León, J., Licandro, J., Serra-Ricart, M., et al. 2019, Research Notes of the American Astronomical Society, 3, 131
Delbo', M., Walsh, K., Bolin, B., Avdellidou, C., & Morbidelli, A. 2017, Science, 357, 1026
Di Sisto, R. P. & Rossignoli, N. L. 2020, arXiv e-prints, arXiv:2006.09657
Do, A., Tucker, M. A., & Tonry, J. 2018, ApJL , 855, L10
Dones, L., Brasser, R., Kaib, N., & Rickman, H. 2015, Space Sci. Rev. , 197, 191
Dones, L., Levison, H., Duncan, M., & Weissman, P. 2000, in AAS/Division for Planetary Sciences Meeting Abstracts, Vol. 32, AAS/Division for Planetary Sciences Meeting Abstracts #32, 36.02
Dones, L., Weissman, P. R., Levison, H. F., & Duncan, M. J. 2004a, in Astronomical Society of the Pacific Conference Series, Vol. 323, Star Formation in the Interstellar Medium: In Honor of David Hollenbach, ed. D. Johnstone, F. C. Adams, D. N. C. Lin, D. A. Neufeeld, & E. C. Ostriker, 371
Dones, L., Weissman, P. R., Levison, H. F., & Duncan, M. J. 2004b, Oort cloud formation and dynamics, ed. M. C. Festou, H. U. Keller, & H. A. Weaver, 153
Drimmel, R. 2000, A&A , 358, L13
Duncan, M., Quinn, T., & Tremaine, S. 1987, AJ , 94, 1330
Duncan, M. J., Babcock, C., Kaib, N., & Levison, H. 2011, in AAS/Division of Dynamical Astronomy Meeting #42, AAS/Division of Dynamical Astronomy Meeting, 9.03
Duncan, M. J., Levison, H. F., & Budd, S. M. 1995, AJ , 110, 3073
Edgeworth, K. E. 1943, Journal of the British Astronomical Association, 53, 181
Elliot, J. L., Kern, S. D., Clancy, K. B., et al. 2005, AJ , 129, 1117
Emel'yanenko, V. V. 2020, A&A , 642, L20
Emery, J. P., Marzari, F., Morbidelli, A., French, L. M., & Grav, T. 2015, The Complex History of Trojan Asteroids, 203–220
Emsenhuber, A., Mordasini, C., Burn, R., et al. 2020a, arXiv e-prints, arXiv:2007.05561
Emsenhuber, A., Mordasini, C., Burn, R., et al. 2020b, arXiv e-prints, arXiv:2007.05562
Engelhardt, T., Jedicke, R., Vereš, P., et al. 2017, AJ , 153, 133
Farrés, A., Laskar, J., Blanes, S., et al. 2013, Celestial Mechanics and Dynamical Astronomy, 116, 141
Fernandez, J. A. 1981, A&A , 96, 26

Fernández, J. A. 1997, Icarus , 129, 106
Fernández, J. A. & Brunini, A. 2000, Icarus , 145, 580
Fernández, J. A., Gallardo, T., & Brunini, A. 2004, Icarus , 172, 372
Fernandez, J. A. & Ip, W. H. 1981, Icarus , 47, 470
Fouchard, M., Emel'yanenko, V., & Higuchi, A. 2020, Celestial Mechanics and Dynamical Astronomy, 132, 43
Fouchard, M., Froeschlé, C., Matese, J. J., & Valsecchi, G. B. 2006a, Celestial Mechanics and Dynamical Astronomy, 96, 341
Fouchard, M., Froeschlé, C., Valsecchi, G., & Rickman, H. 2006b, Celestial Mechanics and Dynamical Astronomy, 95, 299
Fouchard, M., Higuchi, A., Ito, T., & Maquet, L. 2018, A&A , 620, A45
Fouchard, M., Rickman, H., Froeschlé, C., & Valsecchi, G. B. 2013, Icarus , 222, 20
Fouchard, M., Rickman, H., Froeschlé, C., & Valsecchi, G. B. 2014a, Icarus , 231, 110
Fouchard, M., Rickman, H., Froeschlé, C., & Valsecchi, G. B. 2014b, Icarus , 231, 99
Fritz, J., Bitsch, B., Kührt, E., et al. 2014, Planet. Space Sci., 98, 254
Fujii, M., Iwasawa, M., Funato, Y., & Makino, J. 2007, Publ. Astr. Soc. Japan , 59, 1095
Fukushima, H. & Yajima, H. 2021, arXiv e-prints, arXiv:2104.10892
Gardner, E., Nurmi, P., Flynn, C., & Mikkola, S. 2011, MNRAS , 411, 947
Gavagnin, E., Bleuler, A., Rosdahl, J., & Teyssier, R. 2017, MNRAS , 472, 4155
Gerhard, O. 2011, Memorie della Societa Astronomica Italiana Supplementi, 18, 185
Gladman, B., Kavelaars, J. J., Petit, J.-M., et al. 2001, AJ , 122, 1051
Gladman, B., Marsden, B. G., & Vanlaerhoven, C. 2008, Nomenclature in the Outer Solar System, ed. M. A. Barucci, H. Boehnhardt, D. P. Cruikshank, A. Morbidelli, & R. Dotson, 43
Glaser, J. P., McMillan, S. L. W., Geller, A. M., Thornton, J. D., & Giovinazzi, M. R. 2020, AJ , 160, 126
Gomes, R., Levison, H. F., Tsiganis, K., & Morbidelli, A. 2005, Nat , 435, 466
Gomes, R. S., Morbidelli, A., & Levison, H. F. 2004, Icarus , 170, 492
Goodman, J., Heggie, D. C., & Hut, P. 1993, ApJ , 415, 715
Grazier, K. R., Newman, W. I., Kaula, W. M., & Hyman, J. M. 1999, Icarus , 140, 341
Gropp, W. 2002, MPICH2: A New Start for MPI Implementations, ed. D. Kranzlmüller, J. Volkert, P. Kacsuk, & J. Dongarra (Berlin, Heidelberg: Springer Berlin Heidelberg), 7–7
Gropp, W., Lusk, E., Doss, N., & Skjellum, A. 1996, Parallel Computing, 22, 789
Hands, T. O. & Dehnen, W. 2020, MNRAS , 493, L59
Hands, T. O., Dehnen, W., Gration, A., Stadel, J., & Moore, B. 2019, MNRAS , 490, 21
Hanse, J., Jílková, L., Portegies Zwart, S. F., & Pelupessy, F. I. 2018, MNRAS , 473, 5432
Hartmann, W. K. 1965, Icarus , 4, 157
Hartmann, W. K. 1966, Icarus , 5, 406
Hayashi, C., Nakazawa, K., & Nakagawa, Y. 1985, in Protostars and Planets II, ed. D. C. Black & M. S. Matthews, 1100–1153
Heisler, J. & Tremaine, S. 1986, Icarus , 65, 13
Higuchi, A. & Kokubo, E. 2015, AJ , 150, 26
Higuchi, A. & Kokubo, E. 2020, MNRAS , 492, 268
Higuchi, A., Kokubo, E., Kinoshita, H., & Mukai, T. 2007, AJ , 134, 1693
Hill, G. W. 1913, AJ , 27, 171
Hills, J. G. 1981, AJ , 86, 1730
Hills, J. G. 1984, Nat , 311, 636
Hunter, J. D. 2007, Computing in Science and Engineering, 9, 90
Hut, P. 1984, Nat , 311, 638
Ida, S., Larwood, J., & Burkert, A. 2000, ApJ , 528, 351
Ito, T. & Higuchi, A. 2020, in AAS/Division for Planetary Sciences Meeting Abstracts, Vol. 52, AAS/Division for Planetary Sciences Meeting Abstracts, 304.07
Ito, T. & Ohtsuka, K. 2019, Monographs on Environment, Earth and Planets, 7, 1
Ito, T. & Tanikawa, K. 2002, MNRAS , 336, 483
Jetsu, L. & Pelt, J. 2000, A&A , 353, 409
Jewitt, D. C. 2002, AJ , 123, 1039
Jílková, L., Carraro, G., Jungwiert, B., & Minchev, I. 2012, A&A , 541, A64
Jílková, L., Hamers, A., Hammer, M., & Portegies Zwart, S. 2016, MNRAS , 457, 4218
Jílková, L., Portegies Zwart, S., Pijloo, T., & Hammer, M. 2015, MNRAS , 453, 3157
Jiménez-Torres, J. J. 2020, Acta Astron. , 70, 53
Johansen, A. & Lambrechts, M. 2017, Annual Review of Earth and Planetary Sciences, 45, 359
Johansen, A., Oishi, J. S., Mac Low, M.-M., et al. 2007, Nat , 448, 1022
Johansen, A., Ronnet, T., Bizzarro, M., et al. 2021, arXiv e-prints, arXiv:2102.08611
Johnstone, D., Hollenbach, D., & Bally, J. 1998, ApJ , 499, 758
Jurić, M., Ivezić, Ž., Brooks, A., et al. 2008, ApJ , 673, 864
Kaib, N. A. & Quinn, T. 2008, Icarus , 197, 221
Kaib, N. A., Raymond, S. N., & Duncan, M. 2013, Nat , 493, 381
Kaib, N. A., Roskar, R., & Quinn, T. 2011a, in AAS/Division of Dynamical Astronomy Meeting #42, AAS/Division of Dynamical Astronomy Meeting, 9.04
Kaib, N. A., Roškar, R., & Quinn, T. 2011b, Icarus , 215, 491
Kavelaars, J. J., Lawler, S. M., Bannister, M. T., & Shankman, C. 2020, Perspectives on the distribution of orbits of distant Trans-Neptunian objects, ed. D. Prialnik, M. A. Barucci, & L. Young, 61–77
Kenyon, S. J. & Bromley, B. C. 2006, AJ , 131, 1837
Kobayashi, H., Ida, S., & Tanaka, H. 2005, Icarus , 177, 246
Kokubo, E. & Ida, S. 1998, Icarus, 131, 171
Kokubo, E. & Ida, S. 2002, The Astrophysical Journal, 581, 666
Korycansky, D. G. & Papaloizou, J. C. B. 1995, MNRAS , 274, 85
Kozai, Y. 1962, AJ , 67, 591
Kroupa, P. 2001, MNRAS , 322, 231
Kruijer, T. S., Burkhardt, C., Budde, G., & Kleine, T. 2017, Proceedings of the National Academy of Science, 114, 6712
Kuiper, G. P. 1951, in 50th Anniversary of the Yerkes Observatory and Half a Century of Progress in Astrophysics, ed. J. A. Hynek, 357
Lada, C. J. & Lada, E. A. 2003, ARA&A , 41, 57
Laskar, J. 1990, Icarus , 88, 266
Laskar, J., Fienga, A., Gastineau, M., & Manche, H. 2011, A&A , 532, A89
Laughlin, G. & Adams, F. C. 1998, ApJL , 508, L171
Lecar, M., Franklin, F. A., Holman, M. J., & Murray, N. J. 2001, ARA&A , 39, 581
Leto, G., Jakubík, M., Paulech, T., Neslušan, L., & Dybczyński, P. A. 2008, MNRAS , 391, 1350
Leto, G., Jakubík, M., Paulech, T., Neslušan, L., & Dybczyński, P. A. 2009, Earth Moon and Planets, 105, 263
Levison, H. F., Dones, L., & Duncan, M. J. 2001, AJ , 121, 2253
Levison, H. F., Duncan, M. J., Brasser, R., & Kaufmann, D. E. 2010a, Science, 329, 187
Levison, H. F., Morbidelli, A., Van Laerhoven, C., Gomes, R., & Tsiganis, K. 2008, Icarus , 196, 258
Levison, H. F., Thommes, E., & Duncan, M. J. 2010b, AJ , 139, 1297
Li, J., Zhou, L.-Y., & Sun, Y.-S. 2006, Chinese J. Astron. Astrophys., 6, 588
Licht, A. L. 1999, Icarus , 137, 355
Lidov, M. 1962, Planet. Space Sci., 9, 719
Lineweaver, C. H. 2010, in Astrobiology Science Conference 2010: Evolution and Life: Surviving Catastrophes and Extremes on Earth and Beyond, Vol. 1538, 5226
Lüghausen, F., Parmentier, G., Pflamm-Altenburg, J., & Kroupa, P. 2012, MNRAS , 423, 1985
Luhman, K. L. 2014, ApJ , 781, 4
Luu, J. X. & Jewitt, D. C. 2002, ARA&A , 40, 63
Lykawka, P. S. & Mukai, T. 2008, AJ , 135, 1161
Madigan, A.-M. & McCourt, M. 2016, MNRAS , 457, L89
Malhotra, R. 1993, Nat , 365, 819
Malhotra, R. 1998, in American Astronomical Society Meeting Abstracts, Vol. 193, American Astronomical Society Meeting Abstracts, 96.02
Malhotra, R. 2019, Geoscience Letters, 6, 12
Martínez-Barbosa, C. A., Brown, A. G. A., Boekholt, T., et al. 2016, MNRAS , 457, 1062
Martínez-Barbosa, C. A., Brown, A. G. A., & Portegies Zwart, S. 2015, MNRAS , 446, 823
Martínez-Barbosa, C. A., Jílková, L., Portegies Zwart, S., & Brown, A. G. A. 2017, MNRAS , 464, 2290
McKee, C. F. & Ostriker, E. C. 2007, ARA&A , 45, 565
Melott, A. L. & Bambach, R. K. 2010, MNRAS , 407, L99
Milani, A. & Nobili, A. M. 1992, Nat , 357, 569
Miller, R. H. 1964, ApJ , 140, 250
Monari, G., Helmi, A., Antoja, T., & Steinmetz, M. 2014, A&A , 569, A69
Moore, N. W. H., Li, G., & Adams, F. C. 2020, ApJ , 901, 92
Morbidelli, A., Brasser, R., Tsiganis, K., Gomes, R., & Levison, H. F. 2009, A&A , 507, 1041
Morbidelli, A. & Levison, H. F. 2004, AJ , 128, 2564
Morbidelli, A., Levison, H. F., Tsiganis, K., & Gomes, R. 2005, Nat , 435, 462
Morbidelli, A. & Nesvorný, D. 2020, Kuiper belt: formation and evolution, ed. D. Prialnik, M. A. Barucci, & L. Young, 25–59
Morbidelli, A., Tsiganis, K., Crida, A., Levison, H. F., & Gomes, R. 2007, AJ , 134, 1790
Movshovitz, N., Bodenheimer, P., Podolak, M., & Lissauer, J. J. 2010, Icarus , 209, 616
Murray, N. & Holman, M. 1999, Science, 283, 1877
Murray, N. & Holman, M. 2001, Nat , 410, 773
Mustill, A. J., Raymond, S. N., & Davies, M. B. 2016, MNRAS , 460, L109
Napier, K. J., Adams, F. C., & Batygin, K. 2021a, The Planetary Science Journal, 2, 53

Napier, K. J., Gerdes, D. W., Lin, H. W., et al. 2021b, arXiv e-prints, arXiv:2102.05601
Neslušan, L. 2000, A&A , 361, 369
Neslušan, L., Dybczyński, P. A., Leto, G., Jakubík, M., & Paulech, T. 2009, Earth Moon and Planets, 105, 257
Nesvorný, D. 2020, Research Notes of the American Astronomical Society, 4, 212
Neukum, G., Ivanov, B. A., & Hartmann, W. K. 2001, Space Sci. Rev. , 96, 55
Newton, I. 1687, Philosophiae Naturalis Principia Mathematica, Vol. 1
Nordlander, T., Rickman, H., & Gustafsson, B. 2017, A&A , 603, A112
Nurmi, P., Valtonen, M. J., Zheng, J. Q., & Rickman, H. 2002, MNRAS , 333, 835
Offner, S. S. R. & Arce, H. G. 2015, ApJ , 811, 146
Oliphant, T. E. 2006, A guide to NumPy, Vol. 1 (Trelgol Publishing USA)
Oort, J. H. 1950, Bul. Astron. Inst. Neth. , 11, 91
Öpik, E. 1932, Proceedings of the American Academy of Arts and Sciences, 67, 169
Opitom, C., Fitzsimmons, A., Jehin, E., et al. 2019, A&A , 631, L8
'Oumuamua ISSI Team, Bannister, M. T., Bhandare, A., et al. 2019, Nature Astronomy, 3, 594
Parker, R. J. 2020, Royal Society Open Science, 7, 201271
Patterson, C. & Smith, A. B. 1987, Nat , 330, 248
Paulech, T., Jakubík, M., Neslušan, L., Dybczyński, P. A., & Leto, G. 2010, A&A , 509, A48
Pelupessy, F. I., Jänes, J., & Portegies Zwart, S. 2012, New Astron. , 17, 711
Perets, H. B. & Kouwenhoven, M. B. N. 2012, ApJ , 750, 83
Pfalzner, S., Aizpuru Vargas, L., Bhandare, A., & Veras, D. 2021, arXiv e-prints, arXiv:2104.06845
Pfalzner, S., Davies, M. B., Kokaia, G., & Bannister, M. T. 2020, ApJ , 903, 114
Pfalzner, S. & Vincke, K. 2020, ApJ , 897, 60
Pfalzner, S., Vogel, P., Scharwächter, J., & Olczak, C. 2005, A&A , 437, 967
Pirani, S., Johansen, A., Bitsch, B., Mustill, A. J., & Turrini, D. 2018, in AAS/Division for Planetary Sciences Meeting Abstracts, Vol. 50, AAS/Division for Planetary Sciences Meeting Abstracts #50, 200.01D
Pirani, S., Johansen, A., Bitsch, B., Mustill, A. J., & Turrini, D. 2019, A&A , 623, A169
Plummer, H. C. 1911, MNRAS , 71, 460
Popovas, A., Nordlund, Å., Ramsey, J. P., & Ormel, C. W. 2018, MNRAS , 479, 5136
Portegies Zwart, S. 2019, A&A , 622, A69
Portegies Zwart, S. 2020, Nature Astronomy, 4, 819
Portegies Zwart, S. 2021, A&A , 647, A136
Portegies Zwart, S. & McMillan, S. 2018, Astrophysical Recipes; The art of AMUSE
Portegies Zwart, S., McMillan, S., Harfst, S., et al. 2009, New Astronomy, 14, 369
Portegies Zwart, S., Pelupessy, I., Martínez-Barbosa, C. van Elteren, A., & McMillan, S. 2020, Communications in Nonlinear Science and Numerical Simulation, 105240
Portegies Zwart, S., Torres, S., Pelupessy, I., Bédorf, J., & Cai, M. X. 2018, MNRAS , 479, L17
Portegies Zwart, S., van Elteren, A., Pelupessy, I., et al. 2018, AMUSE: the Astrophysical Multipurpose Software Environment
Portegies Zwart, S. F. 2009, ApJL , 696, L13
Portegies Zwart, S. F. & Boekholt, T. C. N. 2018, Communications in Nonlinear Science and Numerical Simulations, 61, 160
Portegies Zwart, S. F. & Jílková, L. 2015, MNRAS , 451, 4663
Portegies Zwart, S. F., McMillan, S. L. W., & Gieles, M. 2010, ARA&A , 48, 431
Portegies Zwart, S. F. & Verbunt, F. 1996, A&A , 309, 179
Punzo, D., Capuzzo-Dolcetta, R., & Portegies Zwart, S. 2014, MNRAS , 444, 2808
Rabinowitz, D. L., Barkume, K., Brown, M. E., et al. 2006, ApJ , 639, 1238
Rampino, M. R. & Prokoph, A. 2020, Astrobiology, 20, 1097
Raup, D. M. & Sepkoski, J. J. 1984, Proceedings of the National Academy of Science, 81, 801
Rawiraswattana, K., Hubber, D. A., & Goodwin, S. P. 2016, MNRAS , 460, 3505
Rein, H. & Liu, S.-F. 2012, A&A , 537, A128
Rein, H. & Spiegel, D. S. 2015, MNRAS , 446, 1424
Rickman, H. 2014, Meteoritics and Planetary Science, 49, 8
Rickman, H., Fouchard, M., Froeschlé, C., & Valsecchi, G. B. 2008, Celestial Mechanics and Dynamical Astronomy, 102, 111
Rickman, H., Kamel, L., Festou, M. C., & Froeschle, C. 1987, in ESA Special Publication, Vol. 278, Diversity and Similarity of Comets, ed. E. J. Rolfe, B. Battrick, M. Ackerman, M. Scherer, & R. Reinhard, 471–481
Romero-Gómez, M., Athanassoula, E., Antoja, T., & Figueras, F. 2011, MNRAS , 418, 1176
Ryder, G. 2002, Journal of Geophysical Research (Planets), 107, 5022
Saillenfest, M. 2020, Celestial Mechanics and Dynamical Astronomy, 132, 12
Saillenfest, M., Fouchard, M., Ito, T., & Higuchi, A. 2019, A&A , 629, A95
Schlecker, M., Mordasini, C., Emsenhuber, A., et al. 2020, arXiv e-prints, arXiv:2007.05563
Scott, D. 1992, Multivariate Density Estimation: Theory, Practice, and Visualization (Wiley Series in Probability and Statistics, John Wiley & Sons, Inc. 1992)
Shankman, C., Gladman, B., & Kaib, N. 2011, in EPSC-DPS Joint Meeting 2011, Vol. 2011, 633
Shannon, A., Jackson, A. P., & Wyatt, M. C. 2019, MNRAS , 485, 5511
Sheppard, S. S., Trujillo, C., & Williams, G. V. 2014, Minor Planet Electronic Circulars, 2014-F40
Sheppard, S. S., Trujillo, C. A., Tholen, D. J., & Kaib, N. 2019, AJ , 157, 139
Siraj, A. & Loeb, A. 2020, ApJL , 899, L24
Sosa, A. & Fernández, J. A. 2009, MNRAS , 393, 192
Sosa, A. & Fernández, J. A. 2011, MNRAS , 416, 767
Stevenson, D. J. & Lunine, J. I. 1988, Icarus , 75, 146
Stock, K., Cai, M. X., Spurzem, R., Kouwenhoven, M. B. N., & Portegies Zwart, S. 2020, MNRAS , 497, 1807
Stöffler, D. & Ryder, G. 2001, Space Sci. Rev. , 96, 9
Sussman, G. J. & Wisdom, J. 1988, Science, 241, 433
Sussman, G. J. & Wisdom, J. 1992, Science, 257, 56
Tanikawa, K. & Ito, T. 2007, Publ. Astr. Soc. Japan , 59, 989
Tegler, S. C. & Romanishin, W. 2000, Nat , 407, 979
Thommes, E., Nagasawa, M., & Lin, D. N. C. 2008, ApJ , 676, 728
Todorović, N., Wu, D., & Rosengren, A. J. 2020, Science Advances, 6, eabd1313
Toomre, A. 1964, ApJ , 139, 1217
Toonen, S., Hamers, A., & Portegies Zwart, S. 2016, Computational Astrophysics and Cosmology, 3, 6
Torres, S. 2020, PhD thesis: Dynamics of the Oort Cloud and the Formation of Interstellar Comets (Leiden Observatory)
Torres, S., Cai, M. X., Brown, A. G. A., & Portegies Zwart, S. 2019, A&A , 629, A139
Torres, S., Cai, M. X., Mukherjee, D., Portegies Zwart, S., & Brown, A. G. A. 2020a, Astron. Astrophys., submitted, 17
Torres, S., Portegies Zwart, S., & Brown, A. G. A. 2020b, Astron. Astrophys., submitted, 10
Trujillo, C. A., Jewitt, D. C., & Luu, J. X. 2000, ApJL , 529, L103
Trujillo, C. A. & Sheppard, S. S. 2014, Nat , 507, 471
Tsiganis, K., Gomes, R., Morbidelli, A., & Levison, H. F. 2005, Nat , 435, 459
Valtonen, M., Mylläri, A., Orlov, V., & Rubinov, A. 2004, in Astronomical Society of the Pacific Conference Series, Vol. 316, Order and Chaos in Stellar and Planetary Systems, ed. G. G. Byrd, K. V. Kholshevnikov, A. A. Myllri, I. I. Nikiforov, & V. V. Orlov, 45
Valtonen, M. J. & Innanen, K. A. 1982, ApJ , 255, 307
Valtonen, M. J., Zheng, J.-Q., & Mikkola, S. 1992, Celestial Mechanics and Dynamical Astronomy, 54, 37
van Rossum, G. 1995, Extending and embedding the Python interpreter, Report CS-R9527
Varadi, F., Runnegar, B., & Ghil, M. 2003, ApJ , 592, 620
Vargya, D. & Sanderson, R. 2020, in AAS/Division of Dynamical Astronomy Meeting, Vol. 52, AAS/Division of Dynamical Astronomy Meeting, 200.05
Veras, D., Evans, N. W., Wyatt, M. C., & Tout, C. A. 2014, MNRAS , 437, 1127
Veras, D., Reichert, K., Flammini Dotti, F., et al. 2020, MNRAS , 493, 5062
Veras, D. & Tout, C. A. 2012, MNRAS , 422, 1648
Veras, D., Wyatt, M. C., Mustill, A. J., Bonsor, A., & Eldridge, J. J. 2011, MNRAS , 417, 2104
Vincke, K., Breslau, A., & Pfalzner, S. 2015, A&A , 577, A115
Vincke, K. & Pfalzner, S. 2016, ApJ , 828, 48
Vokrouhlický, D., Nesvorný, D., & Dones, L. 2019, AJ , 157, 181
Volk, K. & Malhotra, R. 2017, AJ , 154, 62
von Zeipel, H. 1910, Astronomische Nachrichten, 183, 345
Walsh, K. J., Morbidelli, A., Raymond, S. N., O'Brien, D. P., & Mandell, A. M. 2011, Nat , 475, 206
Wang, L., Spurzem, R., Aarseth, S., et al. 2015, MNRAS , 450, 4070
Weissman, P. R. 1983, A&A , 118, 90
Weissman, P. R. 1996, in Astronomical Society of the Pacific Conference Series, Vol. 107, Completing the Inventory of the Solar System, ed. T. Rettig & J. M. Hahn, 265–288
Williams, J. P. & Cieza, L. A. 2011, ARA&A , 49, 67
Winter, A. J., Clarke, C. J., Rosotti, G., et al. 2018, MNRAS , 478, 2700
Wong, E. W., Brasser, R., & Werner, S. C. 2019, Earth and Planetary Science Letters, 506, 407
Wyatt, M. C. 2003, ApJ , 598, 1321
Wyatt, M. C. 2008, ARA&A , 46, 339
Xiang-Gruess, M. 2016, MNRAS , 455, 3086
Zderic, A. & Madigan, A.-M. 2020, AJ , 160, 50
Zellner, N. E. B. 2017, Origins of Life and Evolution of the Biosphere, 47, 261
Zhang, Q. 2018, ApJL , 852, L13
Zheng, J.-Q., Valtonen, M. J., & Valtaoja, L. 1990, Celestial Mechanics and Dynamical Astronomy, 49, 265
Zink, J. K., Batygin, K., & Adams, F. C. 2020, AJ , 160, 232